Entropy generation of tangent hyperbolic nanofluid over a circular cylinder in the presence of nonlinear Boussinesq approximation : a non-similar solution

Basha, HT, Sivaraj, R, Prasad, VR and Beg, OA

http://dx.doi.org/10.1007/s10973-020-09981-5

Journal of Thermal Analysis and Calorimetry manuscript No.
(will be inserted by the editor)

Entropy generation of tangent hyperbolic nanofluid flow over a circular cylinder in the presence of nonlinear Boussinesq approximation: A non-similar solution

H. Thameem Basha[1] · **R. Sivaraj**[1*] · **V. Ramachandra Prasad**[1] · **O.Anwar Beg**[2]

Received: date / Accepted: date

Abstract The analysis of entropy generation has received notable attention in the study of nanofluids because the prime objective of nanofluids is to admit high heat fluxes. The entropy production can be utilized to generate the entropy in any irreversible heat transfer process which is important in thermal machines. This work presents to explore the fluid transport characteristics and entropy generation of a tangent hyperbolic nanofluid over a horizontal circular cylinder with the influence of nonlinear Boussinesq approximation. The dimensionless nonlinear partial differential equations have been solved by using an implicit finite difference Keller box scheme. The impacts of active parameters on the flow field like Weissenberg number, power-law index, magnetic field, mixed convection, Brownian motion, thermal convention, thermophoresis and radiation are illustrated with graphs and tables. The current results exposed that the nanofluid velocity enhances for enhancing the mixed convection parameter. Higher values of nonlinear thermal convection parameter declines the thermal boundary thickness. Total entropy generation decreases for higher values of Eckert number. Isotherms thickness is escalated with increasing values of radiation parameter.

Keywords Tangent hyperbolic nanofluid · entropy generation · nonlinear Boussinesq approximation · inclined magnetic field · Keller box method.

R. Sivaraj
E-mail: sivaraj.kpm@gmail.com
[1]Department of Mathematics, School of Advanced Sciences, Vellore Institute of Technology, Vellore–632014, India

[2]Fluid Mechanics, Aeronautical and Mechanical Engineering Department, School of Computing, Science and Engineering, University of Salford, Manchester M54WT, UK

Nomenclature

a	radius of the cylinder
B_0	strength of the constant magnetic field
Br	Brinkman number
C	concentration of the fluid
C_f^*	skin friction coefficient
$(C_p)_f$	specific heat of fluid
C_W	concentration at the surface
C_∞	ambient concentration
D_B	Brownian diffusion
D_T	thermophoretic diffusion
E_c	Eckert number
g	acceleration due to gravity
k_a	mean absorption coefficient
k_f	fluid thermal conductivity
L_T	diffusion parameter
M_a	magnetic parameter
n_a	power law index
N_B	Brownian motion parameter
N_c	thermal convection parameter
N_G	total entropy generation
N_r	buoyancy ratio parameter
N_T	thermophoresis parameters
Nu^*	Nusselt number
Pr	Prandtl number
R_a	radiation parameter
Re	Reynolds number
Sc	Schmidt number
Sh^*	Sherwood number
S_G	dimensional entropy
T	temperature of fluid
T_W	temperature at the surface
T_∞	ambient temperature
u^*, v^*	velocity components in $x,\ y$ directions
u_e^*	external flow velocity
U_∞	free stream velocity
We	Weissenberg number
x, y	Cartesian coordinates

Greek symbols

α_C	concentration difference parameter
α_T	temperature difference parameter

β_0	coefficient of linear thermal expansion
β_1	coefficient of nonlinear thermal expansion
Γ	material constant
λ_c	mixed convection parameter
μ_f	dynamic viscosity
ρ_f	density of fluid
ρ_p	density of particle
σ	electrical conductivity
σ_B	Stefan Boltzmann constant
τ	ratio between particle and base fluid
Ψ	angle for applied magnetic field

1 Introduction

In recent times, the demand for optimal and efficient energy systems is increasing due to the over exploitation of energy resources. The entropy generation can be utilized to examine the efficiency of the thermodynamic performance of energy systems. The concept of entropy generation was initiated by Bejan [1] by employing the basic laws of thermodynamics, heat transfer process and fluid mechanics. Generally, convective (free, forced, mixed) heat transfer phenomena is related to two types of losses. The first type of loss is caused by the heat transfer through a fixed temperature difference and the second type of loss happens as a consequence of pressure drop in working fluids. These losses are jointly associated with a single property called entropy generation. In other words, an entropy generation is the measure of spices disorder of an energy system. However, several factors like MHD, Joule heating, and diffusion may contribute to irreversibilities which opens the gateway to enhance the thermal efficiency through entropy generation. Ali et al. [2] investigated the entropy generation of chemically reacting Cross nanofluid over a stretched surface with linear radiation and noticed that higher values of Brinkman number and Lorentz force decrease the Bejan number. Sheikholeslami and Ganji [3] employed Koo-Kleinstreuer-Li correlation model to analyze the entropy generation of CuO-water nanofluid in a square enclosure and found that the entropy generation enhances with an increment in nanoparticle volume fraction. Khan et al. [4] numerically scrutinized the stagnation point flow of a Carreau nanofluid with entropy generation and observed that the raising values of diffusive variable augment the entropy generation and Bejan number. Further studies on entropy generation can be found in Refs [5-14].

Fluids which can express the shear stress and shear rate dependent viscosity are classified as non-Newtonian fluids. Biological materials (blood, saliva), chemical materials (polymer fluids, pharmaceutical chemicals), food stuffs (ketchup, yogurt), flow in journal bearings and solar collectors are the examples of the non-Newtonian fluids which find immense applications in biomedical, engineering and technology. The conventional form of Navier-Stokes equations

is not sufficient to elucidate the flow characteristics of non-Newtonian fluids because of complex rheological properties of non-Newtonian fluids. To overcome this shortcoming, many researchers had proposed several rheological models for non-Newtonian fluids such as Cross fluid, Carreau fluid, Maxwell fluid, Walters B-fluid, Casson fluid and Williamson fluid. Several authors investigated different types of non-Newtonian models in various aspects [15-22]. The hyperbolic tangent fluid is one of the subclasses of non-Newtonian fluids which shows shear thinning characteristics (the viscosity of the fluid is decayed as the shear rate amplifies). Compare to other non-Newtonian fluids, tangent hyperbolic fluid has a lot of advantages like computational easiness, physical robustness, and simplicity. Several experimental results reveal that the tangent hyperbolic fluid model has expressed the exact characteristics of the shear-thinning phenomenon. Moreover, this fluid model accurately expresses the rheological properties of blood flow. The hyperbolic tangent fluid has received notable attention because it is used to analyze the blood flow through a tapered artery and fallopian tube. Gaffar et al. [23] employed a non-similar solution to investigate the heat transfer characteristics of hyperbolic tangent fluid with the convective heating surface and noticed that the hyperbolic tangent fluid temperature enhances with an increment in Weissenberg number. Khan et al.[24] utilized Buongiorno nanofluid model to explore the entropy generation and fluid transport properties of tangent hyperbolic nanofluid over a sheet and found that the skin friction factor increases for increasing Weissenberg number. Nayak et al. [25] examined the importance of activation energy on tangent hyperbolic nanofluid flow over a permeable Riga plate by means of thermophoresis and Brownian motion.

In several engineering and industrial manufacturing process, the difference between the wall and ambient temperatures need not to be small. When the temperature difference is notable, the fluid transport properties are significantly affected. In this case, considering the linear Boussinesq approximation in the fluid transport equation is incapable which leads to reduce the quality of the results. Therefore, it is essential to consider the nonlinear Boussinesq approximation in such cases which certainly contributes to improve the accuracy of the results. It is important to mention that the nonlinear Boussinesq approximation should not be used in low-temperature difference cases. In addition, engineering, geophysical and astrophysical flows are the relevant examples of this nonlinear heat convection (Boussinesq approximation). Vasu et al. [26] discussed entropy generation in the time-dependent mixed convective flow of a nanofluid in the presence of nonlinear Boussinesq approximation and noticed that the uplifting convection parameter increases the nanofluid velocity. Mahanthesh et al. [27] explored the impacts on nonlinear convection and non-linear radiation on Maxwell nanofluid over a three-dimensional extending sheet and observed that the x-axis velocity shows an increasing nature for higher values of mixed convection parameter. Waqas et al. [28] used Buongiorno nanofluid to manifest the heat and mass transfer characteristics of magneto-thixotropic nanofluid with an impact of nonlinear convection

and pointed out that the growing values of the thermophoresis parameter inflate the nanofluid temperature and concentration. Patil et al. [29] scrutinized the hydrogen and oxygen diffusion in nanofluid flow over a roughness cone using triple nonlinear convection and observed that the skin friction factor has an oscillating nature for increasing values of roughness surface parameter. Kameswaran et al. [30] modeled and analyzed the nonlinear convection impact on the boundary layer flow over a permeable plate and noticed that the rising values of the nonlinear temperature parameter tend to decline the thickness of the thermal related boundary layer. The term nanofluid was originated by Choi and Eastman [31] and this fluid is acquired by the dilute suspension of nanometer (1-100 nm)-size solid particles in regular fluids (oil, water etc.). It is observed that the heat transfer efficiency of ordinary fluids is highly enhanced with the inclusion of particles like ZnO, Cu, SiO_2, TiO_2, CuO and Al_2O_3[32-36]. Numerous models have been yielded by researchers to look into the nanofluids, in which the Tiwari and Das model and Buongiorno model are notable. The Tiwari and Das [37] model proposes the behavior of nanofluid with the use of solid volume fraction. In the nanofluid, a nonhomogeneous symmetrical model of four equations of two-components for fluid transport using the influence of slip mechanisms (thermophoresis and Brownian movement) was proposed by Buongiorno [38].

To the best of the authors knowledge, no effort has been made to explore the entropy analysis on hyperbolic tangent nanofluid with nonlinear Boussinesq approximation over a circular cylinder. So, the prime intention of the present model is to exhibit the fluid flow and heat transfer characteristics of hyperbolic tangent nanofluid over a horizontal circular cylinder in existence of nonlinear convection. It is noticed that the mixed convection flow of non-Newtonian nanofluid over a heated horizontal cylinder has notable uses in the geological and industrial process such as geothermal reservoirs, thermal recovery of oil, drag reduction, coating of wires, thrust bearing, underground nuclear waste storage sites and assessment of aquifers. The system of fluid transport equations is solved numerically by using unconditionally stable implicit finite difference Keller box method. Influence of diverse pertinent parameters on the velocity, temperature, concentration and entropy generation are analyzed through the graphs.

2 Mathematical Formulation

The schematic view of geometry for the present problem is manifested in Figure 1 which is modeled in a two-dimensional Cartesian coordinate system. The magnetic field strength is assumed to be uniform and is applied parallel to the fluid motion. The coordinates x and y are taken along the circumference of the cylinder and normal to the cylinder, respectively. a is the radius of the cylinder. Changes in density for the buoyancy term is determined by employing nonlinear Boussinesq approximation. The constant temperature (T_W) and

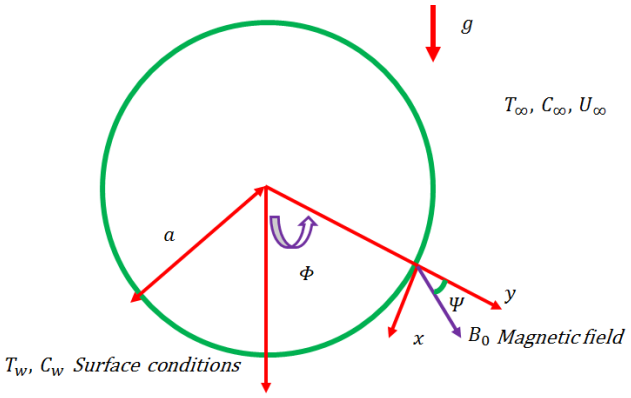

Fig. 1 Physical configuration of the geometry.

concentration (C_W) of the wall is presumed to be greater than the ambient temperature (T_∞) and ambient concentration (C_∞), respectively. Buongiorno nanofluid model is employed to express the momentum, energy and concentration equations. In addition, the following assumptions are taken into consideration.

- Laminar, steady, incompressible, mixed convective flow of tangent hyperbolic nanofluid over a circular cylinder is considered.
- The body force is implemented in the momentum equation.
- The induced magnetic field strength is smaller compared to external magnetic field, so it is neglected.
- Tangent hyperbolic nanofluid dissipation and Joule heating are considered in the energy equation.

Based on these assumptions, the flow of tangent hyperbolic nanofluid is governed by the following equations [4, 15, 23, 26 and 27]

$$\frac{\partial u^*}{\partial x} + \frac{\partial v^*}{\partial y} = 0, \tag{1}$$

$$u^*\frac{\partial u^*}{\partial x} + v^*\frac{\partial u^*}{\partial y} = u_e^*\frac{du_e^*}{dx} + \nu_f\,(1-n_a)\,\frac{\partial^2 u^*}{\partial y^2} + \nu_f\,n_a\,\Gamma\sqrt{2}\left(\frac{\partial u^*}{\partial y}\right)\frac{\partial^2 u^*}{\partial y^2}$$
$$+\left[(1-C_\infty)\,\rho_f\,\beta_0 g\,(T-T_\infty) + (1-C_\infty)\,\rho_f\,\beta_1 g(T-T_\infty)^2\right]\sin\left(\frac{x}{a}\right),$$
$$-g\,(\rho_p-\rho_f)\,(C-C_\infty)\sin\left(\frac{x}{a}\right) - \frac{\sigma B_0^2}{\rho_f}\sin^2\Psi\,(u^*-u_e^*) \tag{2}$$

$$u^*\frac{\partial T}{\partial x} + v^*\frac{\partial T}{\partial y} = \frac{k_f}{(\rho C_p)_f}\frac{\partial^2 T}{\partial y^2} + \tau\left[D_B\frac{\partial C}{\partial y}\frac{\partial T}{\partial y} + \frac{D_T}{T_\infty}\left(\frac{\partial T}{\partial y}\right)^2\right]$$
$$+\frac{\mu_f}{(\rho C_p)_f}\,(1-n_a)\left(\frac{\partial u^*}{\partial y}\right)^2 + \frac{\mu_f}{(\rho C_p)_f}\frac{n_a\Gamma}{\sqrt{2}}\frac{\partial u^*}{\partial y}\left(\frac{\partial u^*}{\partial y}\right)^2$$

$$-\frac{1}{(\rho C_p)_f}\frac{\partial q_r}{\partial y}+\frac{\sigma B_0^2}{(\rho C_p)_f}\sin^2\Psi\ (u^*)^2, \tag{3}$$

$$u^*\frac{\partial C}{\partial x}+v^*\frac{\partial C}{\partial y}=D_B\frac{\partial^2 C}{\partial y^2}+\frac{D_T}{T_\infty}\frac{\partial^2 T}{\partial y^2}. \tag{4}$$

The boundary conditions of this model are as follows

$$\left.\begin{array}{ll} u^*=0,\ v^*=0,\ T=T_W,\ C=C_W & \text{at y}=0,\\ u^*\to u_e^*,\quad T\to T_\infty,\quad C\to C_\infty & \text{as}\quad \text{y}\to\infty. \end{array}\right\} \tag{5}$$

According to Rashad et al. [39], external flow (u_e^*) of the fluid transport equation can be expresses as u_e^* =sin $\left(\frac{x}{a}\right)U_\infty$.

The radiative heat flux [27] is expressed as

$$q_r=-\frac{4}{3}\frac{\sigma_B}{k_a}\left(\frac{\partial T^4}{\partial y}\right)=-\frac{16}{3}\frac{\sigma_B T_\infty^3}{k_a}\left(\frac{\partial T}{\partial y}\right), \tag{6}$$

Suitable non-similarity variables are expressed as follows

$$\left.\begin{array}{l} \xi=\frac{x}{a},\eta=\sqrt{\text{Re}}\left(\frac{y}{a}\right),u=\frac{u^*}{U_\infty},\ v=\sqrt{\text{Re}}\left(\frac{v^*}{U_\infty}\right),\ u_e\left(\xi\right)=\frac{u_e^*(x)}{U_\infty},\\ T=T_\infty+\theta\left(T_W-T_\infty\right),\quad C=C_\infty+\phi\left(C_W-C_\infty\right). \end{array}\right\} \tag{7}$$

where $\text{Re}=\frac{aU_\infty}{\nu_f}$.

By implementing the above variables, Eqns. (1)-(4) are transformed as

$$\frac{\partial u}{\partial\xi}+\frac{\partial v}{\partial\eta}=0, \tag{8}$$

$$u\frac{\partial u}{\partial\xi}+v\frac{\partial u}{\partial\eta}=u_e\frac{du_e}{d\xi}+\left(1-n_a\right)\frac{\partial^2 u}{\partial\eta^2}+n_aWe\frac{\partial u}{\partial\eta}\frac{\partial^2 u}{\partial\eta^2}$$
$$-M_a\sin^2\Psi\left(u-u_e\right)+\lambda_c\left(\theta+N_c\theta^2-N_r\phi\right)\sin\xi, \tag{9}$$

$$u\frac{\partial\theta}{\partial\xi}+v\frac{\partial\theta}{\partial\eta}=\frac{1}{\text{Pr}}\left(1+\frac{4}{3}R_a\right)\frac{\partial^2\theta}{\partial\eta^2}+N_B\frac{\partial\theta}{\partial\eta}\frac{\partial\phi}{\partial\eta}+N_T\left(\frac{\partial\theta}{\partial\eta}\right)^2$$
$$+M_aE_c\sin^2\Psi(u)^2+E_c\left(1-n_a\right)\left(\frac{\partial u}{\partial\eta}\right)^2+E_c\frac{n_aWe}{2}\frac{\partial u}{\partial\eta}\left(\frac{\partial u}{\partial\eta}\right)^2, \tag{10}$$

$$u\frac{\partial\phi}{\partial\xi}+v\frac{\partial\phi}{\partial\eta}=\frac{1}{Sc}\left[\frac{\partial^2\phi}{\partial\eta^2}+\frac{N_T}{N_B}\frac{\partial^2\theta}{\partial\eta^2}\right]. \tag{11}$$

with the corresponding boundary conditions

$$\left.\begin{array}{ll} u=0,\ v=0,\ \theta=1,\ \phi=1 & \text{at}\ \eta=0,\\ u\to u_e,\quad \theta\to 0,\quad \phi\to 0 & \text{as}\quad \eta\to\infty. \end{array}\right\} \tag{12}$$

where $\lambda_c=\frac{(1-C_\infty)g\beta_0(T_W-T_\infty)a}{U_\infty^2}$, $We=\frac{\Gamma\sqrt{\text{Re}}\sqrt{2}\,U_\infty}{a}$, $\text{Pr}=\frac{\nu_f}{\alpha^*}$, $M_a=\frac{\sigma B_0^2 a}{U_\infty\rho_f}$, $N_c=\frac{\beta_1(T_W-T_\infty)}{\beta_0}$, $N_r=\frac{(\rho_p-\rho_f)(C_W-C_\infty)}{(1-C_\infty)\rho_f\beta_0(T_W-T_\infty)}$, $E_c=\frac{U_\infty^2}{(C_p)_f(T_W-T_\infty)}$, $N_B=$

$\frac{\tau D_B(C_W-C_\infty)}{\nu_f}$, $R_a=\frac{4\sigma_B T_\infty^3}{k_a k_f}$, $N_T=\frac{\tau D_B(T_W-T_\infty)}{\nu_f T_\infty}$ and $Sc=\frac{\nu_f}{D_B}$.

To expresses the flow equations with the boundary conditions in dimensionless form, $\psi=\xi f(\xi,\eta)$, $\theta=\theta(\xi,\eta)$, $\phi=\phi(\xi,\eta)$ are assumed according to Rashad et al. [39], where ψ is the stream function which is defined as $u=\frac{\partial(\psi(\xi,\eta))}{\partial\eta}$ & $v=-\frac{\partial(\psi(\xi,\eta))}{\partial\xi}$.

$$(1-n_a)f'''+n_aWef'''f''+ff''-(f')^2+\frac{\sin\xi\cos\xi}{\xi}-M_a\sin^2\Psi\left(1-\frac{\sin\xi}{\xi}\right)+\lambda_c\frac{\sin\xi}{\xi}\left(\theta+N_c\theta^2-N_r\phi\right)=\xi\left[f'\frac{\partial f'}{\partial\xi}-f''\frac{\partial f}{\partial\xi}\right], \quad (13)$$

$$\frac{1}{\Pr}\left[1+\frac{4}{3}R_a\right]\theta''+f\theta'+N_B\theta'\phi'+N_T(\theta')^2+E_c\xi^2M\sin^2\Psi(f')^2+E_c\xi^2(1-n_a)(f'')^2+E_c\xi^3n_a\frac{We}{2}(f'')^3=\xi\left[f'\frac{\partial\theta}{\partial\xi}-\theta'\frac{\partial f}{\partial\xi}\right], \quad (14)$$

$$\frac{1}{Sc}\left[\phi''+\frac{N_T}{N_B}\theta''\right]+f\phi'=\xi\left[f'\frac{\partial\phi}{\partial\xi}-\phi'\frac{\partial f}{\partial\xi}\right]. \quad (15)$$

along with the transformed boundary conditions

$$\left.\begin{array}{llll} f=f'=0, & \theta=\phi=1 & \text{at } \eta=0, \\ f'\to 1, & \theta\to 0, \quad \phi\to 0 & \text{as } \eta\to\infty. \end{array}\right\} \quad (16)$$

Table 1 Comparison result of Nu^* for various values of ξ with Pr=0.71, $R_a=0$, M_a=0.5, Sc=0.6, We=u_e=N_r=E_c=n_a=N_B=N_T=N_c=0,$\Psi=90^\circ$

ξ	$Nu^*(Gr)^{-1/4}=-\theta'(\xi,0)$			
	Merkin[40]	Yih[41]	Prasad et al.[22]	Present
0.0	0.4212	0.4214	0.4211	0.4211
0.2	0.4204	0.4207	0.4206	0.4206
0.4	0.4182	0.4184	0.4185	0.4185
0.6	0.4145	0.4147	0.4146	0.4146
0.8	0.4093	0.4096	0.4095	0.4095
1.0	0.4025	0.4030	0.4027	0.4027

At the wall, the dimensionless forms of skin friction factor $\left(C_f^*\right)$, heat transfer rate (Nu^*) and mass transfer rate (Sh^*) are defined as

$$\left.\begin{array}{l} C_f^*\left(Gr^{-3/4}\right)=(1-n_a)\xi f''(\xi,0)+\frac{n_a}{2}We\xi(f''(\xi,0))^2, \\ Nu^*\left(Gr^{-1/4}\right)=-\left(1+\frac{4}{3}R_a\right)\theta'(\xi,0), \\ Sh^*\left(Gr^{-1/4}\right)=-\phi'(\xi,0). \end{array}\right\} \quad (17)$$

2.1 **Entropy generation**

The dimensional form of entropy generation for nanofluid can be written as follows [22 and 24]:

$$S_G = \underbrace{\frac{k_f}{{T_\infty}^2}\left(1+\frac{16\sigma_B T_\infty^3}{3k_f k_a}\right)\left(\frac{\partial T}{\partial y}\right)^2}_{\text{Thermal irreversibility}} + \underbrace{\frac{RD}{C_\infty}\left(\frac{\partial C}{\partial y}\right)^2 + \frac{RD}{T_\infty}\left(\frac{\partial T}{\partial y}\frac{\partial C}{\partial y}\right)}_{\text{Mass irreversibility}} + \underbrace{\frac{\mu_f}{T_\infty}\left[(1-n_a)\left(\frac{\partial u^*}{\partial y}\right)^2 + \frac{n_a\Gamma}{\sqrt{2}}\frac{\partial u^*}{\partial y}\left(\frac{\partial u^*}{\partial y}\right)^2\right]}_{\text{Tangent hyperbolic nanofluid friction irreversibility}} + \underbrace{\frac{\sigma}{T_\infty}B_0^2\sin^2\Psi(u^*)^2}_{\text{Joule heating irreversibility}}, \tag{18}$$

where, D is the mass diffusivity and R is the constant.

Using Eqn. (7) in Eqn. (18), the transformed expression for entropy generation is

$$\begin{aligned} N_G = {} & \alpha_T\left(1+\tfrac{4}{3}R_a\right)\left(\frac{\partial\theta}{\partial\eta}\right)^2 + Br\,(1-n_a)\left(\frac{\partial u}{\partial\eta}\right)^2 + Br\,\frac{n_a We}{2}\frac{\partial u}{\partial\eta}\left(\frac{\partial u}{\partial\eta}\right)^2 \\ & + M_a Br\sin^2\Psi(u)^2 + L_T\left(\frac{\alpha_C}{\alpha_T}\right)\left(\frac{\partial\phi}{\partial\eta}\right)^2 + L_T\frac{\partial\theta}{\partial\eta}\frac{\partial\phi}{\partial\eta}, \end{aligned} \tag{19}$$

where $N_G = \frac{S_G T_\infty a}{k_f(T_W - T_\infty)\mathrm{Re}}$, $\alpha_T = \frac{T_W - T_\infty}{T_\infty}$, $\alpha_C = \frac{C_W - C_\infty}{C_\infty}$, $L_T = \frac{RD(C_W - C_\infty)}{k_f}$ and $Br = \frac{\mu_f U_\infty^2}{k_f(T_W - T_\infty)}$.

Employing ψ, θ and ϕ function for dimensionless form of total entropy generation

$$\begin{aligned} N_G = {} & \alpha_T\left(1+\tfrac{4}{3}R_a\right)(\theta')^2 + Br\xi^2(1-n_a)(f'')^2 + Br\xi^3\,\frac{n_a We}{2}(f'')^3 \\ & + M_a Br\xi^2\sin^2\Psi(f')^2 + L_T\left(\frac{\alpha_C}{\alpha_T}\right)(\phi')^2 + L_T\theta'\phi'. \end{aligned} \tag{20}$$

Further, Bejan number is expressed as the ratio between entropy generation due to heat and mass transfer and total entropy generation

$$Be = \frac{\alpha_T\left(1+\frac{4}{3}R_a\right)(\theta')^2 + L_T\left(\frac{\alpha_C}{\alpha_T}\right)(\phi')^2 + L_T\theta'\phi'}{\left.\begin{array}{l} \alpha_T\left(1+\frac{4}{3}R_a\right)(\theta')^2 + Br\xi^2(1-n_a)(f'')^2 \\ + Br\xi^3\,\frac{n_a We}{2}(f'')^3 + M_a Br\xi^2\sin^2\Psi(f')^2 \\ + L_T\left(\frac{\alpha_C}{\alpha_T}\right)(\phi')^2 + L_T\theta'\phi' \end{array}\right\} = N_G} \tag{21}$$

Table 2 Impacts of n_a and N_c on local skin friction coefficient $\left(C_f^*\right)$, dimensionless local rate of heat transfer (Nu^*) and dimensionless local rate of mass transfer for various values of ξ.

Physical Parameters	Values	Physical Quantities	ξ						CPU time(Sec.)
			0	0.2	0.4	0.6	0.8	1	
n_a	0.1	C_f^*	0	0.3803	0.7283	1.0230	1.2482	1.3938	10.848590
		Nu^*	1.1063	1.0954	1.0738	1.0421	1.0010	0.9514	
		Sh^*	0.8271	0.8201	0.8061	0.7853	0.7578	0.7239	
	0.3	C_f^*	0	0.3672	0.7013	0.9810	1.1906	1.3208	11.069575
		Nu^*	1.1097	1.0992	1.0783	1.0475	1.0075	0.9589	
		Sh^*	0.8291	0.8225	0.8093	0.7897	0.7636	0.7314	
	0.5	C_f^*	0	0.3542	0.6744	0.9393	1.1334	1.2482	11.046161
		Nu^*	1.1132	1.1031	1.0829	1.0530	1.0139	0.9664	
		Sh^*	0.8314	0.8252	0.8127	0.7940	0.7693	0.7387	
	0.8	C_f^*	0	0.3348	0.6346	0.8777	1.0487	1.1401	11.207880
		Nu^*	1.1188	1.1092	1.0899	1.0612	1.0236	0.9777	
		Sh^*	0.8354	0.8296	0.8180	0.8008	0.7779	0.7495	
N_c	0.1	C_f^*	0	0.3672	0.7013	0.9810	1.1906	1.3208	10.820276
		Nu^*	1.1097	1.0992	1.0783	1.0475	1.0075	0.9589	
		Sh^*	0.8291	0.8225	0.8093	0.7897	0.7636	0.7314	
	0.5	C_f^*	0	0.4042	0.7741	1.0876	1.3280	1.4855	11.010522
		Nu^*	1.1257	1.1154	1.0949	1.0647	1.0254	0.9779	
		Sh^*	0.8469	0.8405	0.8279	0.8090	0.7841	0.7533	
	1.0	C_f^*	0	0.4499	0.8639	1.2189	1.4973	1.6879	11.057783
		Nu^*	1.1445	1.1343	1.1142	1.0845	1.0459	0.9994	
		Sh^*	0.8674	0.8613	0.8492	0.8312	0.8075	0.7782	
	1.5	C_f^*	0	0.4950	0.9526	1.3485	1.6641	1.8871	10.904997
		Nu^*	1.1620	1.1520	1.1321	1.1028	1.0647	1.0188	
		Sh^*	0.8864	0.8805	0.8689	0.8516	0.8288	0.8006	

3 Numerical method and code validation

The dimensionless equations under the suitable conditions are solved numerically using unconditionally stable implicit finite difference scheme which is known as the Keller box method (KBM). The present numerical scheme is second-order accurate for the boundary layer problem which is represented using parabolic type partial differential equations(PDEs). The procedure to obtain the solution by using the Keller box method is given below

- The n^{th} order dimensionless equations are transformed into n first order dimensionless equations.
- The transformed n first order equations are discretized by employing central differences approach.
- The algebraic equations are linearized by means of Newton's method.
- The results are obtained by using the block matrix system (block tridiagonal elimination technique).

Step 1:

We have considered a new set of variables $u\left(\xi,\eta\right), v\left(\xi,\eta\right), s\left(\xi,\eta\right), t\left(\xi,\eta\right), g\left(\xi,\eta\right), p\left(\xi,\eta\right)$

to transform the n^{th} order dimensionless equations into the first order dimensionless equations, which depends on ξ and η.

$$f = f, f' = u,\ u' = v,\ \theta = s,\ s' = t,\ \phi = g,\ g' = p \tag{22}$$

$$(1-n_a)\,\xi v' + n_a We \xi v' v + f v - u^2 + \frac{\sin\xi\cos\xi}{\xi} - M_a \sin^2\Psi \left(u - \frac{\sin\xi}{\xi}\right) + \lambda_c \frac{\sin\xi}{\xi}\left(s + N_c s^2 - N_r g\right) = \xi\left[u\frac{\partial u}{\partial \xi} - v\frac{\partial f}{\partial \xi}\right], \tag{23}$$

$$\frac{1}{\Pr}\left[1 + \frac{4}{3}R_a\right] t' + N_T\, t^2 + N_B t\, p + M_a E_c \xi^2 \sin^2\Psi (u)^2 + f\, t + E_c\,(1-n_a)\,\xi^2 v^2 + E_c \frac{n_a We}{2}\xi^3 v^3 = \xi\left[u\frac{\partial s}{\partial \xi} - t\frac{\partial f}{\partial \xi}\right], \tag{24}$$

$$\frac{1}{Sc}\left[p' + \frac{N_T}{N_B}t'\right] + fp = \xi\left[u\frac{\partial g}{\partial \xi} - p\frac{\partial f}{\partial \xi}\right]. \tag{25}$$

with the boundary conditions

$$\begin{aligned} &\eta = 0: \quad u = 0, \quad f = 0, \quad s = 1, \quad g = 1 \\ &\eta \to \infty: \quad u \to 1, \quad s = 0, \quad g = 0 \end{aligned} \tag{26}$$

Step 2:
The net point of x and y plane is expressed as

$$\xi^0 = 0, \quad \xi^i = \xi^{i-1} + k_i,\ i = 1, 2, 3...I, \tag{27}$$

$$\eta_0 = 0, \quad \eta_j = \eta_{j-1} + h_j,\ j = 1, 2, 3...J. \tag{28}$$

where k_i is $\Delta\xi$ spacing in the i^{th} node and h_j is $\Delta\eta$ spacing in j^{th} node.

$$\left(\frac{\partial()}{\partial\xi}\right)^{i-\frac{1}{2}}_{j-\frac{1}{2}} = \frac{()^i_{j-\frac{1}{2}} - ()^{i-1}_{j-\frac{1}{2}}}{k_i}, \quad \left(\frac{\partial()}{\partial\eta}\right)^{i-\frac{1}{2}}_{j-\frac{1}{2}} = \frac{()^{i-\frac{1}{2}}_j - ()^{i-\frac{1}{2}}_{j-1}}{h_j}$$

$$()^{i-\frac{1}{2}}_j = \frac{()^{i-1}_j - ()^i_j}{2}, \quad ()^i_{j-\frac{1}{2}} = \frac{()^i_{j-1} - ()^i_j}{2}$$

The midpoint $\left(\xi^i, \eta_{j-\frac{1}{2}}\right)$ is considered between the segments $\left(\xi^i, \eta_{j-1}\right)\left(\xi^i, \eta_j\right)$ by using central difference approximation

$$f' = u \Rightarrow u^i_{j-\frac{1}{2}} = \frac{u^i_j + u^i_{j-1}}{2} = \frac{\left(f^i_j - f^i_{j-1}\right)}{h_j}, \tag{29}$$

$$u' = v \Rightarrow v^i_{j-\frac{1}{2}} = \frac{v^i_j + v^i_{j-1}}{2} = \frac{\left(u^i_j - u^i_{j-1}\right)}{h_j}, \tag{30}$$

$$s' = t \Rightarrow t^i_{j-\frac{1}{2}} = \frac{t^i_j + t^i_{j-1}}{2} = \frac{\left(s^i_j - s^i_{j-1}\right)}{h_j}, \tag{31}$$

$$g' = p \Rightarrow p^i_{j-\frac{1}{2}} = \frac{p^i_j + p^i_{j-1}}{2} = \frac{\left(g^i_j - g^i_{j-1}\right)}{h_j}, \tag{32}$$

First order PDEs Eqns. (23)-(25) are approximated by centering the rectangle points ($P_1, P_2, P_3,$ and P_4) at $\left(\xi^{i-\frac{1}{2}},\, \eta_{j-\frac{1}{2}}\right)$

$$\left.\begin{array}{l} \left(\frac{v^i_j - v^i_{j-1}}{h_j}\right)(1-n_a)\,\xi + n_a We\,\xi\, v^i_{j-1/2}\left(\frac{v^i_j - v^i_{j-1}}{h_j}\right) \\ +(1+\alpha)\left(f^i_{j-1/2} v^i_{j-1/2}\right) - (1+\alpha)\left(u^i_{j-1/2}\right)^2 - \left(M_a \sin^2\Psi\right) u^i_{j-1/2} \\ +M_a \sin^2\Psi 2B + 2H + \lambda_c B\left(s^i_{j-1/2} + N_c\left(s^i_{j-1/2}\right)^2 - N_r g^i_{j-1/2}\right) \\ +\alpha v^{i-1}_{j-1/2} f^i_{j-1/2} - \alpha f^{i-1}_{j-1/2} v^i_{j-1/2} \\ = -\left[\begin{array}{l} \left(\frac{v^i_j - v^i_{j-1}}{h_j}\right)(1-n_a)\,\xi + n_a We\,\xi\, v^i_{j-1/2}\left(\frac{v^i_j - v^i_{j-1}}{h_j}\right) \\ +(1-\alpha)\left(f^{i-1}_{j-1/2} v^{i-1}_{j-1/2}\right) + (\alpha-1)\left(u^{i-1}_{j-1/2}\right)^2 \\ +\lambda_c B\left(s^i_{j-1/2} + N_c\left(s^i_{j-1/2}\right)^2 - N_r g^i_{j-1/2}\right) \\ -\left(M_a \sin^2\Psi\right) u^{i-1}_{j-1/2} \end{array}\right] \end{array}\right\} \tag{33}$$

$$\left.\begin{array}{l} \frac{1}{\Pr}\left[1 + \frac{4}{3}R_a\right]\left(\frac{t^i_j - t^i_{j-1}}{h_j}\right) + N_B\left(t^i_{j-1/2} p^i_{j-1/2}\right) + N_T\left(t^i_{j-1/2}\right)^2 \\ +M_a E_c \sin^2\Psi \xi^2\left(u^i_{j-1/2}\right)^2 + E_c\,(1-n_a)\,\xi^2\left(v^i_{j-1/2}\right)^2 \\ +E_c \frac{n_a We}{2}\xi^3\left(v^i_{j-1/2}\right)^3 - \alpha u^{i-1}_{j-1/2} s^i_{j-1/2} - \alpha f^{i-1}_{j-1/2} t^i_{j-1/2} \\ +\alpha t^{i-1}_{j-1/2} f^i_{j-1/2} + (1+\alpha)\left(f^i_{j-1/2} t^i_{j-1/2}\right) \\ -\alpha\left(u^i_{j-1/2} s^i_{j-1/2}\right) + \alpha s^{i-1}_{j-1/2} u^i_{j-1/2} \\ = -\left[\begin{array}{l} \frac{1}{\Pr}\left[1 + \frac{4}{3}R_a\right]\left(\frac{t^i_j - t^i_{j-1}}{h_j}\right) + N_B\left(t^i_{j-1/2} p^i_{j-1/2}\right) \\ +M_a E_c \sin^2\Psi \xi^2\left(u^i_{j-1/2}\right)^2 + E_c\,(1-n_a)\,\xi^2\left(v^i_{j-1/2}\right)^2 \\ +E_c \frac{n_a We}{2}\xi^3\left(v^i_{j-1/2}\right)^3 + N_T\left(t^i_{j-1/2}\right)^2 \\ +(1-\alpha)\left(f^{i-1}_{j-1/2} t^{i-1}_{j-1/2}\right) + \alpha\left(u^{i-1}_{j-1/2} s^{i-1}_{j-1/2}\right) \end{array}\right] \end{array}\right\} \tag{34}$$

$$\left.\begin{array}{l} \frac{1}{Sc}\left(\frac{p^i_j - p^i_{j-1}}{h_j}\right) + \frac{1}{Sc}\left(\frac{N_T}{N_B}\right)\left(\frac{t^i_j - t^i_{j-1}}{h_j}\right) \\ +(1+\alpha)\left(f^i_{j-1/2} p^i_{j-1/2}\right) - \alpha\left(u^i_{j-1/2} g^i_{j-1/2}\right) + \alpha g^{i-1}_{j-1/2} u^i_{j-1/2} \\ -\alpha u^{i-1}_{j-1/2} g^i_{j-1/2} - \alpha f^{i-1}_{j-1/2} p^i_{j-1/2} + \alpha p^{i-1}_{j-1/2} f^i_{j-1/2} \\ = -\left[\begin{array}{l} \frac{1}{Sc}\left(\frac{p^i_j - p^i_{j-1}}{h_j}\right) + \frac{1}{Sc}\left(\frac{N_T}{N_B}\right)\left(\frac{t^i_j - t^i_{j-1}}{h_j}\right) \\ +(1-\alpha)\left(f^{i-1}_{j-1/2} p^{i-1}_{j-1/2}\right) + \alpha\left(u^{i-1}_{j-1/2} g^{i-1}_{j-1/2}\right) \end{array}\right] \end{array}\right\} \tag{35}$$

where $\alpha = \frac{\xi^{n-1/2}}{k_n}$, $B = \frac{\sin\left(\xi^{n-1/2}\right)}{\xi^{n-1/2}}$ and $H = \frac{\sin\left(\xi^{n-1/2}\right)\cos\left(\xi^{n-1/2}\right)}{\xi^{n-1/2}}$.

subject to the boundary conditions

$$f_0^i = u_0^i = 0,\ s_0^i = 1,\ g_0^i = 1,\ u_J^i \to 1,\ s_J^i = 0,\ g_J^i = 0 \tag{36}$$

Step 3:
The unknowns $(f_j^i,\ u_j^i,\ v_j^i,\ g_j^i,\ p_j^i,\ s_j^i,\ t_j^i)$ are calculated by using the known values of $f_j^{i-1},\ u_j^{i-1}, v_j^{i-1}, g_j^{i-1},\ p_j^{i-1}, s_j^{i-1}, t_j^{i-1}$ where $0 \le \mathrm{j} \le \mathrm{J}$.

The unknowns are assumed as $(f_j^i,\ u_j^i,\ v_j^i,\ g_j^i,\ p_j^i,\ s_j^i,\ t_j^i) \equiv (f_j,\ u_j,\ v_j,\ g_j,\ p_j,\ s_j,\ t_j)$.

The set of central difference equations are expressed as

$$\frac{u_j + u_{j-1}}{2} = \frac{f_j - f_{j-1}}{h_j}, \tag{37}$$

$$\frac{v_j + v_{j-1}}{2} = \frac{u_j - u_{j-1}}{h_j}, \tag{38}$$

$$\frac{t_j + t_{j-1}}{2} = \frac{s_j - s_{j-1}}{h_j}, \tag{39}$$

$$\frac{p_j + p_{j-1}}{2} = \frac{g_j - g_{j-1}}{h_j}, \tag{40}$$

$$\left.\begin{array}{l}
(v_j - v_{j-1})(1-n_a)\xi + n_a We \xi \frac{(v_j+v_{j-1})}{2}(v_j - v_{j-1}) + 2h_j H \\
+\frac{(1+\alpha)h_j}{4}\left[(f_j + f_{j-1})(v_j + v_{j-1})\right] - \frac{h_j}{4}(1+\alpha)(u_j + u_{j-1})^2 \\
-\frac{h_j}{2}\left(M_a \sin^2\Psi\right)(u_j + u_{j-1}) + h_j M_a \sin^2\Psi\ 2B \\
-\frac{\alpha h_j}{2} f_{j-1/2}^{i-1}(v_j + v_{j-1}) + \frac{\alpha h_j}{2} v_{j-1/2}^{i-1}(f_j + f_{j-1}) \\
+\frac{\lambda_c B h_j}{2}\left[(s_j + s_{j-1}) + N_c \frac{(s_j+s_{j-1})^2}{2} - N_r(g_j + g_{j-1})\right] = [E_1]_{j-1/2}^{i-1}
\end{array}\right\} \tag{41}$$

$$\left.\begin{array}{l}
\frac{1}{\mathrm{Pr}}\left[1 + \frac{4}{3}R_a\right](t_j - t_{j-1}) + \frac{N_B}{4} h_j (t_j + t_{j-1})(p_j + p_{j-1}) \\
+\frac{M_a E_c}{4} h_j \sin^2\Psi \xi^2 (u_j + u_{j-1})^2 + \frac{E_c}{4} h_j (1-n_a)\xi^2 (v_j + v_{j-1})^2 \\
+\frac{E_c n_a}{16} We\, h_j \xi^3 (v_j + v_{j-1})^3 + \frac{N_T}{4} h_j (t_j + t_{j-1})^2 \\
+\frac{(1+\alpha)h_j}{4}(f_j + f_{j-1})(t_j + t_{j-1}) - \frac{\alpha h_j}{4}\left[(u_j + u_{j-1})(s_j + s_{j-1})\right] \\
+\frac{\alpha h_j}{2} s_{j-1/2}^{i-1}(u_j + u_{j-1}) - \frac{\alpha h_j}{2} u_{j-1/2}^{i-1}(s_j + s_{j-1}) \\
-\frac{\alpha h_j}{2} f_{j-1/2}^{i-1}(t_j + t_{j-1}) + \frac{\alpha h_j}{2} t_{j-1/2}^{i-1}(f_j + f_{j-1}) = [E_2]_{j-1/2}^{i-1}
\end{array}\right\} \tag{42}$$

$$\left.\begin{array}{l}
\frac{1}{Sc}(p_j - p_{j-1}) + \frac{1}{Sc}\frac{N_T}{N_B}(t_j - t_{j-1}) \\
+\frac{(1+\alpha)h_j}{4}\left[(f_j + f_{j-1})(p_j + p_{j-1})\right] - \frac{\alpha h_j}{4}\left[(u_j + u_{j-1})(g_j + g_{j-1})\right] \\
+\frac{\alpha h_j}{2} g_{j-1/2}^{i-1}(u_j + u_{j-1}) - \frac{\alpha h_j}{2} u_{j-1/2}^{i-1}(g_j + g_{j-1}) \\
-\frac{\alpha h_j}{2} f_{j-1/2}^{i-1}(p_j + p_{j-1}) + \frac{\alpha h_j}{2} p_{j-1/2}^{i-1}(f_j + f_{j-1}) = [E_3]_{j-1/2}^{i-1}
\end{array}\right\} \tag{43}$$

where,

$$[E_1]_{j-1/2}^{i-1} = -h_j \begin{bmatrix} \left(\frac{v_j - v_{j-1}}{h_j}\right)(1-n_a)\,\xi + n_a We \xi v_{j-1/2}\left(\frac{v_j - v_{j-1}}{h_j}\right) \\ +(1-\alpha)\left(f_{j-1/2}v_{j-1/2}\right) + (\alpha-1)\left(u_{j-1/2}\right)^2 \\ +\lambda_c B\left(s_{j-1/2} + N_c\left(s_{j-1/2}\right)^2 - N_r g_{j-1/2}\right) \\ -\left(M_a \sin^2\Psi\right) u_{j-1/2} \end{bmatrix} \tag{44}$$

$$[E_2]_{j-1/2}^{i-1} = -h_j \begin{bmatrix} \frac{1}{\Pr}\left[1 + \frac{4}{3}R_a\right]\left(\frac{t_j - t_{j-1}}{h_j}\right) + N_B\left(t_{j-1/2}p_{j-1/2}\right) \\ +M_a E_c \sin^2\Psi\xi^2\left(u_{j-1/2}\right)^2 + E_c\,(1-n_a)\,\xi^2\left(v_{j-1/2}\right)^2 \\ +E_c\frac{n_a We}{2}\xi^3\left(v_{j-1/2}\right)^3 + N_T\left(t_{j-1/2}\right)^2 \\ +(1-\alpha)\left(f_{j-1/2}t_{j-1/2}\right) + \alpha\left(u_{j-1/2}s_{j-1/2}\right) \end{bmatrix} \tag{45}$$

$$[E_3]_{j-1/2}^{i-1} = -h_j \begin{bmatrix} \frac{1}{Sc}\left(\frac{p_j - p_{j-1}}{h_j}\right) + \frac{1}{Sc}\left(\frac{N_T}{N_B}\right)\left(\frac{t_j - t_{j-1}}{h_j}\right) \\ +(1-\alpha)\left(f_{j-1/2}p_{j-1/2}\right) + \alpha\left(u_{j-1/2}g_{j-1/2}\right) \end{bmatrix} \tag{46}$$

$[E_1]_{j-1/2}^{i-1}$, $[E_2]_{j-1/2}^{i-1}$ and $[E_3]_{j-1/2}^{i-1}$ are the known quantities.

To linearize the nonlinear system of equations using Newtons method, the following iterates are introduced

$$\omega f_j^{(n)} = f_j^{(n+1)} - f_j^{(n)}, \tag{47}$$
$$\omega u_j^{(n)} = u_j^{(n+1)} - u_j^{(n)}, \tag{48}$$
$$\omega v_j^{(n)} = v_j^{(n+1)} - v_j^{(n)}, \tag{49}$$
$$\omega s_j^{(n)} = s_j^{(n+1)} - s_j^{(n)}, \tag{50}$$
$$\omega t_j^{(n)} = t_j^{(n+1)} - t_j^{(n)}, \tag{51}$$
$$\omega g_j^{(n)} = g_j^{(n+1)} - g_j^{(n)}, \tag{52}$$
$$\omega p_j^{(n)} = p_j^{(n+1)} - p_j^{(n)} \tag{53}$$

Implementing the above mentioned expressions in Eqns. (37)-(43) and omitting higher-orders of ω, the following equations are obtained

$$\omega f_j - \omega f_{j-1} - \frac{h_j}{2}\omega u_j - \frac{h_j}{2}\omega u_{j-1} - (e_1)_j = 0 \tag{54}$$
$$\omega u_j - \omega u_{j-1} - \frac{h_j}{2}\omega v_j - \frac{h_j}{2}\omega v_{j-1} - (e_2)_j = 0 \tag{55}$$
$$\omega s_j - \omega s_{j-1} - \frac{h_j}{2}\omega t_j - \frac{h_j}{2}\omega t_{j-1} - (e_3)_j = 0 \tag{56}$$

$$\omega g_j - \omega g_{j-1} - \frac{h_j}{2}\omega p_j - \frac{h_j}{2}\omega p_{j-1} - (e_4)_j = 0 \tag{57}$$

$$\begin{aligned}&(a_1)_j\omega v_j + (a_2)_j\omega v_{j-1} + (a_3)_j\omega f_j + (a_4)_j\omega f_{j-1} + (a_5)_j\omega u_j\\&+(a_6)_j\omega u_{j-1} + (a_7)_j\omega s_j + (a_8)_j\omega s_{j-1}\\&+(a_9)_j\omega g_j + (a_{10})_j\omega g_{j-1} - (e_5)_{j-1/2} = 0,\end{aligned} \tag{58}$$

$$\begin{aligned}&(b_1)_j\omega t_j + (b_2)_j\omega t_{j-1} + (b_3)_j\omega f_j + (b_4)_j\omega f_{j-1}\\&+(b_5)_j\omega u_j + (b_6)_j\omega u_{j-1} + (b_7)_j\omega s_j + (b_8)_j\omega s_{j-1}\\&+(b_9)_j\omega v_j + (b_{10})_j\omega v_{j-1} + (b_{11})_j\omega p_j + (b_{12})_j\omega p_{j-1} = 0\end{aligned} \tag{59}$$

$$\begin{aligned}&(c_1)_j\omega p_j + (c_2)_j\omega p_{j-1} + (c_3)_j\omega f_j + (c_4)_j\omega f_{j-1} + (c_5)_j\omega u_j + (c_6)_j\omega u_{j-1}\\&+(c_7)_j\omega g_j + (c_8)_j\omega g_{j-1} + (c_9)_j\omega t_j + (c_{10})_j\omega t_{j-1} - (e_7)_{j-1/2} = 0,\end{aligned} \tag{60}$$

where,

$$(a_1)_j = (1-n_a)\,\xi + n_a\,We\,\xi v_{j-1/2} + h_j\left[\frac{1+\alpha}{2}f_{j-1/2} - \frac{\alpha}{2}h_j f^{n-1}_{j-1/2}\right],$$

$$(a_2)_j = -(1-n_a)\,\xi - n_a\,We\,\xi v_{j-1/2} + h_j\left[\frac{1+\alpha}{2}f_{j-1/2} - \frac{\alpha}{2}h_j f^{n-1}_{j-1/2}\right],$$

$$(a_3)_j = h_j\left[\frac{(1+\alpha)}{2}v_{j-1/2} + \frac{\alpha}{2}v^{n-1}_{j-1/2}\right],$$

$$(a_4)_j = (a_3)_j,$$

$$(a_5)_j = h_j\left[-(1+\alpha)\,u_{j-1/2} - \frac{M_a}{2}\sin^2\Psi\right],$$

$$(a_6)_j = (a_5)_j,$$

$$(a_7)_j = h_j\frac{\lambda_c\,B}{2} + h_j\,\lambda_c\,B\,N_c\,s_{j-1/2},$$

$$(a_8)_j = (a_7)_j,$$

$$(a_9)_j = -\frac{B}{2}h_j N_r,$$

$$(a_{10})_j = (a_9)_j,$$

$$(b_1)_j = \frac{1}{\Pr}\left[1+\frac{4}{3}R_a\right] + h_j\left[N_T t_{j-1/2} + \frac{N_B}{2}p_{j-1/2} + \frac{1+\alpha}{2}f_{j-1/2} - \frac{\alpha}{2}f^{n-1}_{j-1/2}\right],$$

$$(b_2)_j = -\frac{1}{\Pr}\left[1+\frac{4}{3}R_a\right] + h_j\left[N_T t_{j-1/2} + \frac{N_B}{2}p_{j-1/2} + \frac{1+\alpha}{2}f_{j-1/2} - \frac{\alpha}{2}f^{n-1}_{j-1/2}\right],$$

$$(b_3)_j = h_j\left[\frac{(1+\alpha)}{2}t_{j-1/2} + \frac{\alpha}{2}t^{n-1}_{j-1/2}\right],$$

$$(b_4)_j = (b_3)_j,$$

$$(b_5)_j = h_j\left[M_a\,E_c\sin^2\Psi\,u_{j-1/2} - \frac{\alpha}{2}s_{j-1/2} + \frac{\alpha}{2}s^{n-1}_{j-1/2}\right],$$

$$(b_6)_j = (b_5)_j,$$

$$(b_7)_j = h_j\left[-\frac{\alpha}{2}u_{j-1/2} - \frac{\alpha}{2}u^{n-1}_{j-1/2}\right],$$

$$(b_8)_j = (b_7)_j,$$

$$(b_9)_j = h_j \left[E_c \ (1 - n_a) \ \xi^2 \, v_{j-1/2} + \ \frac{E_c \, n_a \, We}{2} \, \xi^3 \left(v_{j-1/2} \right)^2 \right],$$
$$(b_{10})_j = (b_9)_j$$
$$(b_{11})_j = h_j \left[\frac{N_B}{2} t_{j-1/2} \right],$$
$$(b_{12})_j = h_j \left[\frac{N_B}{2} t_{j-1/2} \right]$$
$$(c_1)_j = \frac{1}{Sc} + h_j \left[\frac{(1+\alpha)}{2} f_{j-1/2} - \frac{\alpha}{2} f^{n-1}_{j-1/2} \right],$$
$$(c_2)_j = -\frac{1}{Sc} + h_j \left[\frac{(1+\alpha)}{2} f_{j-1/2} - \frac{\alpha}{2} f^{n-1}_{j-1/2} \right],$$
$$(c_3)_j = h_j \left[\frac{(1+\alpha)}{2} p_{j-1/2} + \frac{\alpha}{2} p^{n-1}_{j-1/2} \right],$$
$$(c_4)_j = (c_3)_j,$$
$$(c_5)_j = h_j \left[-\frac{\alpha}{2} g_{j-1/2} + \frac{\alpha}{2} g^{n-1}_{j-1/2} \right],$$
$$(c_6)_j = (c_5)_j,$$
$$(c_7)_j = h_j \left[-\frac{\alpha}{2} u_{j-1/2} - \frac{\alpha}{2} u^{n-1}_{j-1/2} \right],$$
$$(c_8)_j = (c_7)_j,$$
$$(c_9)_j = \frac{1}{Sc} \frac{N_T}{N_B},$$
$$(c_{10})_j = -(c_9)_j,$$

$$(e_5)_{j-1/2} = (v_{j-1} - v_j) \left[(1 - n_a) \, \xi + n_a \, We \, \xi v_{j-1/2} \right] - h_j \, (1+\alpha) \, f_{j-1/2}$$
$$v_{j-1/2} + (1+\alpha) \, h_j \left(u_{j-1/2} \right)^2 + M_a \, h_j \sin^2\Psi \, u_{j-1/2} - M_a \sin^2\Psi \, 2 \, B \, h_j$$
$$-2H \, h_j - \lambda_c B \, h_j \left[s_{j-1/2} + N_c \left(s_{j-1/2} \right)^2 - N_r \, g_{j-1/2} \right]$$
$$+\alpha \, h_j \, v_{j-1/2} f^{n-1}_{j-1/2} - \alpha h_j f_{j-1/2} v^{n-1}_{j-1/2} + (E_1)^{i-1}_{j-1/2} \tag{61}$$
$$(e_6)_{j-1/2} = (t_{j-1} - t_j) \left[\frac{1}{\mathrm{Pr}} \left(1 + \frac{4}{3} R_a \right) \right] - N_B h_j t_{j-1/2} p_{j-1/2} - N_T h_j \left(t_{j-1/2} \right)^2$$
$$-h_j M_a \, \xi^2 E_c \sin^2\Psi \left(u_{j-1/2} \right)^2 - E_c \, (1 - n_a) \, \xi^2 h_j \left(v_{j-1/2} \right)^2 - E_c \, n_a \, \frac{We}{2} \xi^3 \, h_j \left(v_{j-1/2} \right)^3$$
$$- (1+\alpha) \, h_j f_{j-1/2} t_{j-1/2} + h_j \alpha u_{j-1/2} s_{j-1/2} - \alpha h_j s^{n-1}_{j-1/2} u_{j-1/2}$$
$$+\alpha h_j u^{n-1}_{j-1/2} s_{j-1/2} + \alpha h_j f^{n-1}_{j-1/2} t_{j-1/2}, - \alpha h_j t^{n-1}_{j-1/2} f_{j-1/2}, \tag{62}$$
$$(e_7)_{j-1/2} = \frac{1}{Sc} \, (p_{j-1} - p_j) - (1+\alpha) \, h_j f_{j-1/2} p_{j-1/2}$$
$$+h_j \alpha u_{j-1/2} g_{j-1/2} - \alpha h_j g^{n-1}_{j-1/2} u_{j-1/2} + \alpha h_j u^{n-1}_{j-1/2} g_{j-1/2} + \alpha h_j f^{n-1}_{j-1/2} p_{j-1/2}$$

$$-\alpha h_j p_{j-1/2}^{n-1} f_{j-1/2} + \left[\frac{1}{Sc}\frac{N_T}{N_B}\right](t_{j-1} - t_j) + (E_3)_{j-1/2}^{i-1}. \tag{63}$$

The boundary conditions Eqn. (36) become

$$\left.\begin{array}{l} \omega f_0 = 0,\ \omega u_0 = 0,\ \omega s_0^n = 0,\ \omega g_0 = 0, \\ \omega u_J = 0,\ \omega s_J = 0,\ \omega g_J = 0,\ f_0^n = u_0^n = 0, \\ s_0^n = 1,\ g_0^n = 1,\ u_J^n = 0,\ s_J^n = 0,\ g_J^n = 0 \end{array}\right\} \tag{64}$$

Step 4:
The block-elimination method is used to compute the linearized difference Eqns. (47)-(56) which is outlined by Cebeci and Pradshaw [42].

$$A\omega = e \tag{65}$$

where,

$$A = \begin{bmatrix} [A_1] & [C_1] & & & & \\ [B_2] & [A_2] & [C_2] & & & \\ & & \ddots & & & \\ & & & \ddots & & \\ & & & & \ddots & \\ & & & & [B_{J-1}] & [A_{J-1}] & [C_{J-1}] \\ & & & & & [B_J] & [C_J] \end{bmatrix}, \tag{66}$$

$$\omega = \begin{bmatrix} [\omega_1] \\ [\omega_2] \\ \\ \vdots \\ \\ [\omega_{J-1}] \\ [\omega_J] \end{bmatrix}, \qquad e = \begin{bmatrix} [e_1] \\ [e_2] \\ \\ \vdots \\ \\ [e_{J-1}] \\ [e_J] \end{bmatrix}. \tag{67}$$

The elements of the matrices are as follows

$$[A_1] = \begin{bmatrix} 0 & 0 & 0 & 1 & 0 & 0 & 0 \\ -\frac{h_j}{2} & 0 & 0 & 0 & -\frac{h_j}{2} & 0 & 0 \\ 0 & -\frac{h_j}{2} & 0 & 0 & 0 & -\frac{h_j}{2} & 0 \\ 0 & 0 & -\frac{h_j}{2} & 0 & 0 & 0 & -\frac{h_j}{2} \\ (a_2)_1 & 0 & 0 & (a_3)_1 & (a_1)_1 & 0 & 0 \\ (b_{10})_1 & (b_{12})_1 & (b_2)_1 & (b_3)_1 & (b_9)_1 & (b_{11})_1 & (b_1)_1 \\ 0 & (c_2)_1 & (c_{10})_1 & (c_3)_1 & 0 & (c_1)_1 & (c_9)_1 \end{bmatrix}, \tag{68}$$

$$[A_J] = \begin{bmatrix} -\frac{h_j}{2} & 0 & 0 & 1 & 0 & 0 & 0 \\ -1 & 0 & 0 & 0 & -\frac{h_j}{2} & 0 & 0 \\ 0 & -1 & 0 & 0 & 0 & -\frac{h_j}{2} & 0 \\ 0 & 0 & -1 & 0 & 0 & 0 & -\frac{h_j}{2} \\ (a_6)_j & (a_{10})_j & (a_8)_j & (a_3)_j & (a_1)_j & 0 & 0 \\ (b_6)_j & 0 & (b_8)_j & (b_3)_j & (b_9)_j & (b_{11})_j & (b_1)_j \\ (c_6)_j & (c_8)_j & 0 & (c_3)_j & 0 & (c_1)_j & (c_9)_j \end{bmatrix}, 2 \le j \le J \tag{69}$$

$$[B_J] = \begin{bmatrix} 0\,0\,0 & -1 & 0 & 0 & 0 \\ 0\,0\,0 & 0 & -\frac{h_j}{2} & 0 & 0 \\ 0\,0\,0 & 0 & 0 & -\frac{h_j}{2} & 0 \\ 0\,0\,0 & 0 & 0 & 0 & -\frac{h_j}{2} \\ 0\,0\,0 & (a_4)_j & (a_2)_j & 0 & 0 \\ 0\,0\,0 & (b_4)_j & (b_{10})_j & (b_{12})_j & (b_2)_j \\ 0\,0\,0 & (c_4)_j & 0 & (c_2)_j & (c_{10})_j \end{bmatrix}, 2 \le j \le J \tag{70}$$

$$[C_J] = \begin{bmatrix} -\frac{h_j}{2} & 0 & 0 & 0\,0\,0\,0 \\ 1 & 0 & 0 & 0\,0\,0\,0 \\ 0 & 1 & 0 & 0\,0\,0\,0 \\ 0 & 0 & 1 & 0\,0\,0\,0 \\ (a_5)_j & (a_9)_j & (a_7)_j & 0\,0\,0\,0 \\ (b_5)_j & 0 & (b_7)_j & 0\,0\,0\,0 \\ (c_5)_j & (c_7)_j & 0 & 0\,0\,0\,0 \end{bmatrix}, \ 1 \le j \le J-1 \tag{71}$$

$$[\omega_1] = \begin{bmatrix} \omega v_0 \\ \omega p_0 \\ \omega t_0 \\ \omega f_1 \\ \omega v_1 \\ \omega p_1 \\ \omega t_1 \end{bmatrix}, \qquad [\omega_j] = \begin{bmatrix} \omega u_{j-1} \\ \omega g_{j-1} \\ \omega s_{j-1} \\ \omega f_j \\ \omega v_j \\ \omega p_j \\ \delta t_j \end{bmatrix}, \ 2 \le j \le J \tag{72}$$

$$\text{and } [e_j] = \begin{bmatrix} (e_1)_{j-(1/2)} \\ (e_2)_{j-(1/2)} \\ (e_3)_{j-(1/2)} \\ (e_4)_{j-(1/2)} \\ (e_5)_{j-(1/2)} \\ (e_6)_{j-(1/2)} \\ (e_7)_{j-(1/2)} \end{bmatrix}, \ 1 \le j \le J \tag{73}$$

In the present problem, we have fastened the ξ and η maximums as 1 and 30, respectively. The difference between the special nodes is taken as 0.05

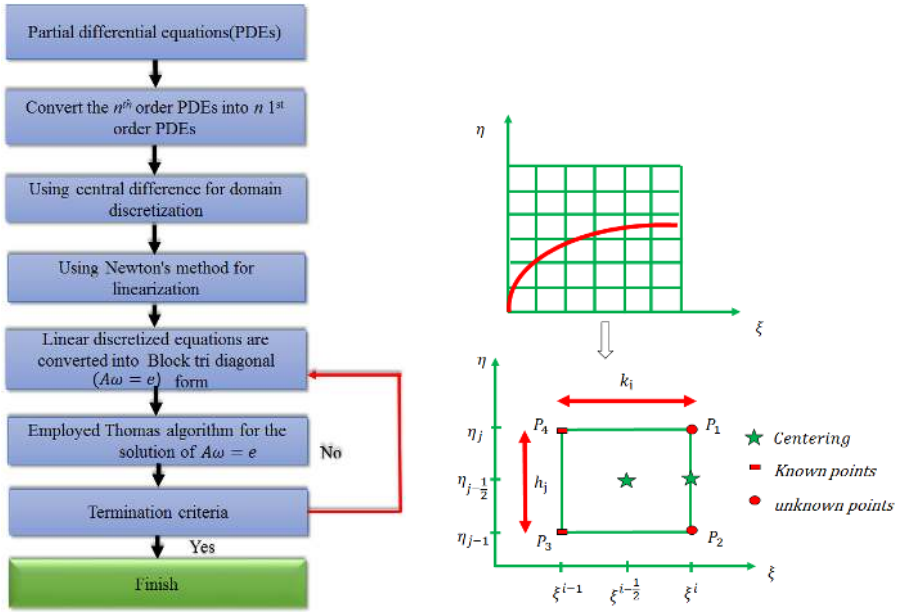

Fig. 2 Solution approach by computer, boundary layer mesh and Keller box element .

in both directions for the solution convergence. It is noteworthy to mention that the parabolic boundary layer is meshed as (20×600). To increase the accuracy of the present solution, the convergence criterion is fixed as 10^{-6} at all gird points. Comparison results of Nu^* for various values of ξ are illustrated in Table 1. It is observed from this table that present results show a good accordance with the results obtained by Merkin [40], Yih[41], and Prasad et al.[22] which depicts that the obtained numerical solution is precise. Tables 2, 3 and 4 manifest the skin friction factor, rate of heat and mass transfer of active parameters. Figure 2 displays the solution approach by computer, boundary layer mesh and Keller box element.

4 Results and discussion

This current section is aimed to visualize the influence of emerging parameters like Weissenberg number ($We = 0, 1, 2, 3$), power law index ($n_a = 0.1, 0.3, 0.5, 0.7$), magnetic field ($M_a = 0.5, 1.0, 1.5, 2.0$), angle of inclination ($\Psi = \frac{\pi}{5}, \frac{\pi}{4}, \frac{\pi}{3}, \frac{\pi}{2}$), mixed convection parameter ($\lambda_c = 1, 3, 7, 10$), Eckert number ($E_c = 0.01, 0.1, 0.3, 0.5$), thermal convention parameter ($N_c = 0.1, 0.5, 1, 1.5$), Brownian motion ($N_B = 0.3, 0.5, 0.7, 0.9$), thermophoresis (N_T=0.01,0.1,0.3,0.5) and radiation (R_a=0.0,0.5,1.0,1.5) on velocity (f'), temperature (θ), concentration (ϕ), skin friction factor (C_f^*), rate of heat transfer (Nu^*) and rate of mass transfer (Sh^*). Dimensionless form of the flow and transport equa-

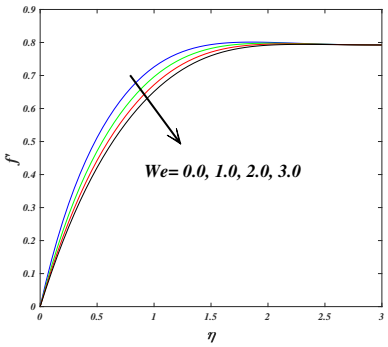

Fig. 3 f' for uplifting values of We.

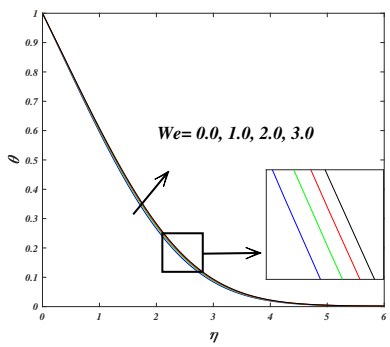

Fig. 4 θ for uplifting values of We.

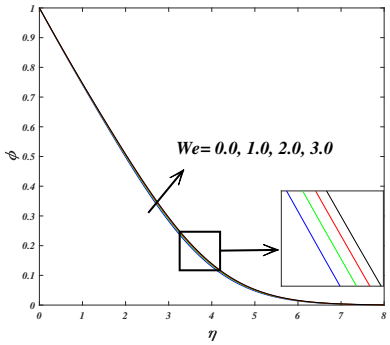

Fig. 5 ϕ for uplifting values of We.

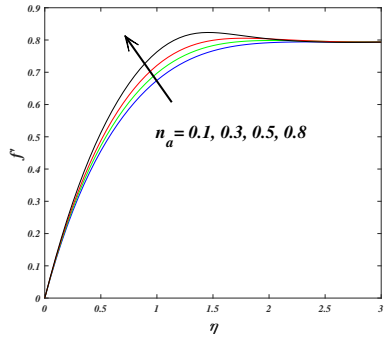

Fig. 6 f' for uplifting values of n_a.

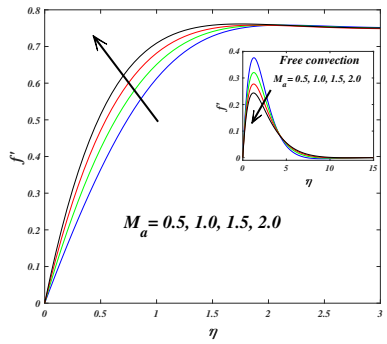

Fig. 7 f' for uplifting values of M_a.

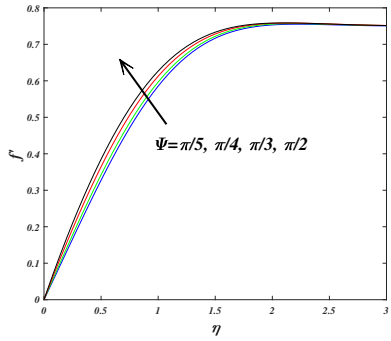

Fig. 8 f' for uplifting values of Ψ.

tions subject to boundary conditions have been computed by KBM. In this computation, the pertinent parameters of tangent hyperbolic nanofluid transport equations are fastened as N_B=0.3, N_T=0.1, R_a=0.5, E_c=0.01, N_r=0.5, Pr=1, Sc=0.3, M_a=0.5, N_a=0.3, We=1.0, $\Psi = \frac{\pi}{3}$, λ_c =1 and N_c=0.1. In en-

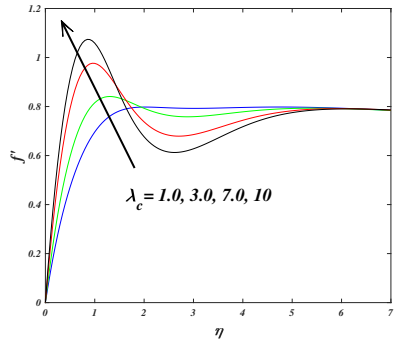

Fig. 9 f' for uplifting values of λ_c.

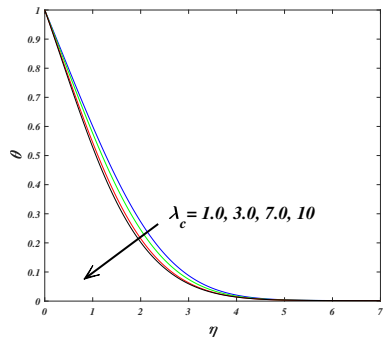

Fig. 10 θ for uplifting values of λ_c.

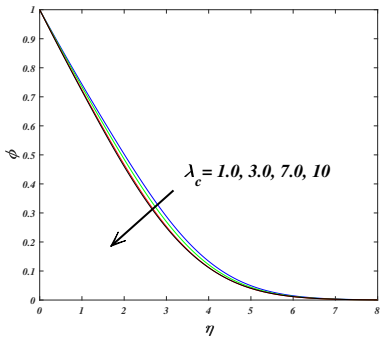

Fig. 11 ϕ for uplifting values of λ_c.

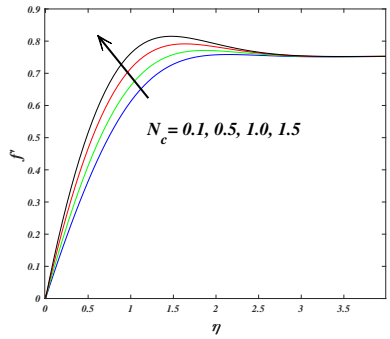

Fig. 12 f' for uplifting values of N_c.

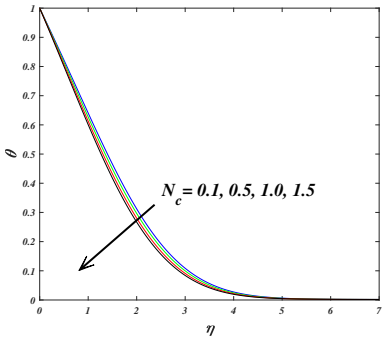

Fig. 13 θ for uplifting values of N_c.

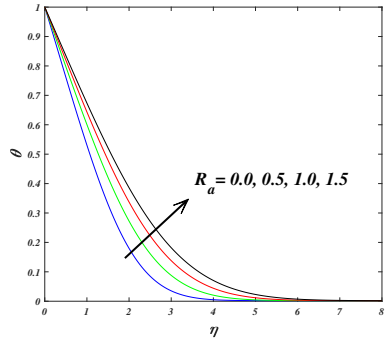

Fig. 14 θ for uplifting values of R_a.

gineering systems, entropy generation has notable applications to model the energy-efficient devices. The entropy generation minimization approach is very important to illustrate the losses in thermo hydraulic systems and engineering systems. Therefore, this analysis can provide a clear view of researchers to en-

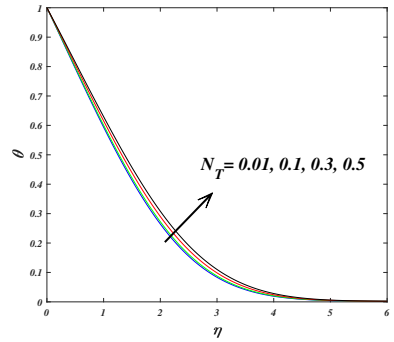

Fig. 15 θ for uplifting values of N_T.

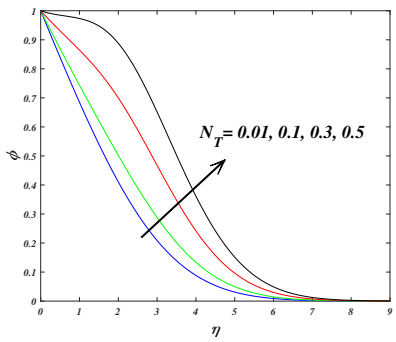

Fig. 16 ϕ for uplifting values of N_T.

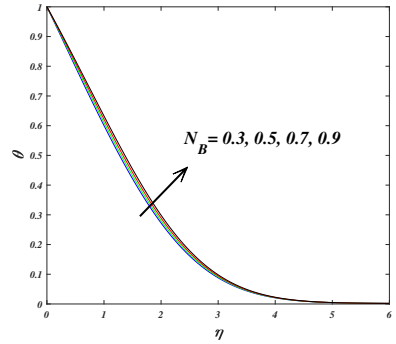

Fig. 17 θ for uplifting values of N_B.

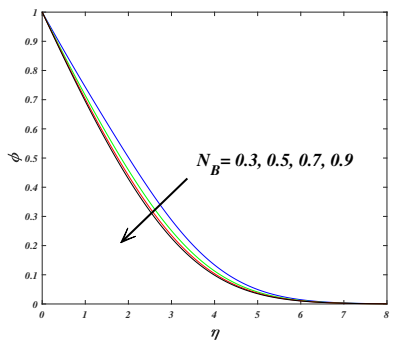

Fig. 18 ϕ for uplifting values of N_B.

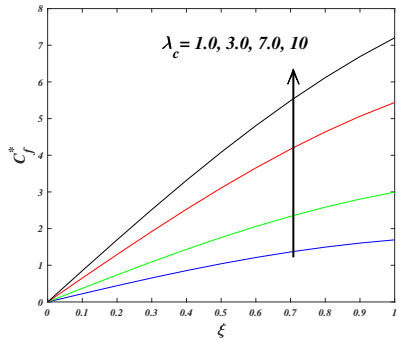

Fig. 19 $C_f{}^*$ for uplifting values of λ_c.

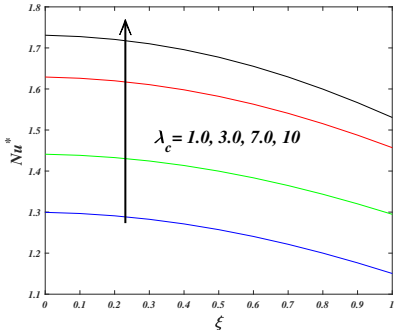

Fig. 20 Nu^* for uplifting values of λ_c.

hance the efficiency of thermal systems. Figures 3-24 depict the characteristics of fluid transport properties, Figs. 25-27 illustrate the streamlines, isotherms and isoconcentrations, and Figs. 28-35 express the entropy generation.

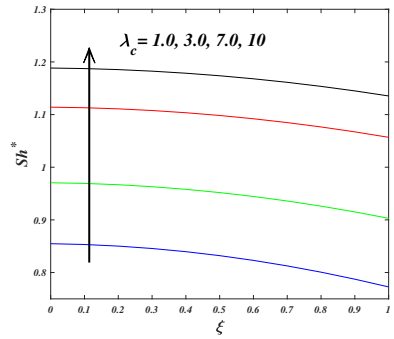

Fig. 21 Sh^* for uplifting values of λ_c.

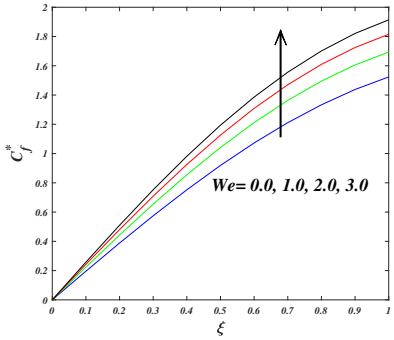

Fig. 22 C_f^* for uplifting values of We.

Figure 3 illustrates the impact of We on tangent hyperbolic nanofluid velocity. We is expressed as the ratio of tangent hyperbolic fluid relaxation time and specific process. It is noticed that the relaxation time of the fluid uplifts by enhancing the We. This generates resistance in the fluid flow direction which diminishes the velocity. Figures 4 and 5 exhibit the behavior of We on temperature and concentration, respectively. From these figures, it is seen that the thermal and mass related boundary layer thicknesses are slightly amplified as We increases. Hence, tangent hyperbolic nanofluid temperature and concentration distributions raise. Figure 6 depicts the impact of n_a on f'. Increasing values of n_a abridge the friction in tangent hyperbolic nanofluid flow which results in uplifting velocity distribution. Impact of M_a on tangent hyperbolic nanofluid velocity is depicted in Fig. 7 for nonlinear mixed convection and free convection cases. In an electrically conductive fluid, the magnetic field acting in the transverse to the geometry creates a resistive force called Lorentz force. It is noteworthy to mention that the Lorentz force has the behavior to prohibit fluid velocity, this nature can be observed in free convection flows. To express the nature of free convection in the present problem, the external force and nonlinear convection in the momentum equation (Eqn. 13) are modified as $(1-n_a)\,f''' + n_a We f''' f'' + f f'' - (f')^2 - M_a \sin^2\Psi \quad + \frac{\sin\xi}{\xi}(\theta - N_r\phi) = \xi\left[f'\frac{\partial f'}{\partial \xi} - f''\frac{\partial f}{\partial \xi}\right]$ and the momentum boundary condition (Eqn. 16) is modified as $f' = 0$ as $\eta \to \infty$. The usual nature of the magnetic field is obtained in free convection flow which is displayed in the subgraph but the velocity profiles uplift with an increase in M_a due to the presence of nonlinear mixed convection. Figure 8 presents the effect of variation of Ψ on nanofluid velocity profiles. It is observed form this figure that direction of the applied magnetic field to the flow shifts from transverse to horizontal for raising the angle of inclination. It is well known that the magnetic field applied in horizontal direction experiences lower Lorentz force compared to vertical direction. In the nonlinear mixed convection flow, fluid velocity elevates for amplifying the an-

gle of inclination.

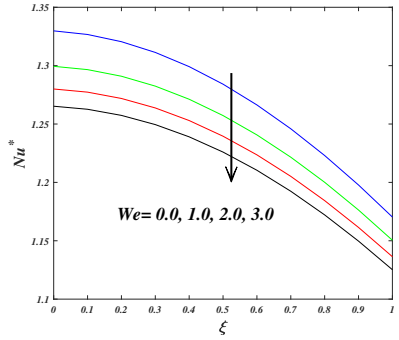

Fig. 23 Nu^* for uplifting values of We.

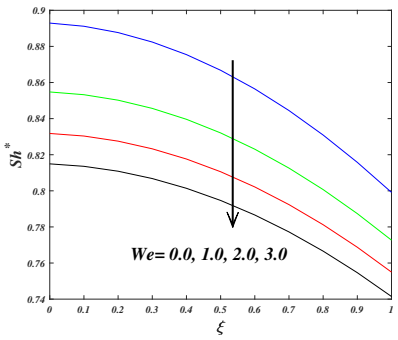

Fig. 24 Sh^* for uplifting values of We.

f', θ and ϕ for several values of λ_c are manifested in Figs. 9-11. It is noteworthy to mention that the positive and negative values of λ_c represent the hot and cold cylinder, respectively. It is seen from Fig. 9 that nanofluid velocity shows an increasing nature near the geometry ($\eta < 2$) for increasing the values of λ_c but the opposite nature is observed in the region $2 < \eta < 5$. It is clear from Figs. 10 and 11 that nanofluid temperature and concentration

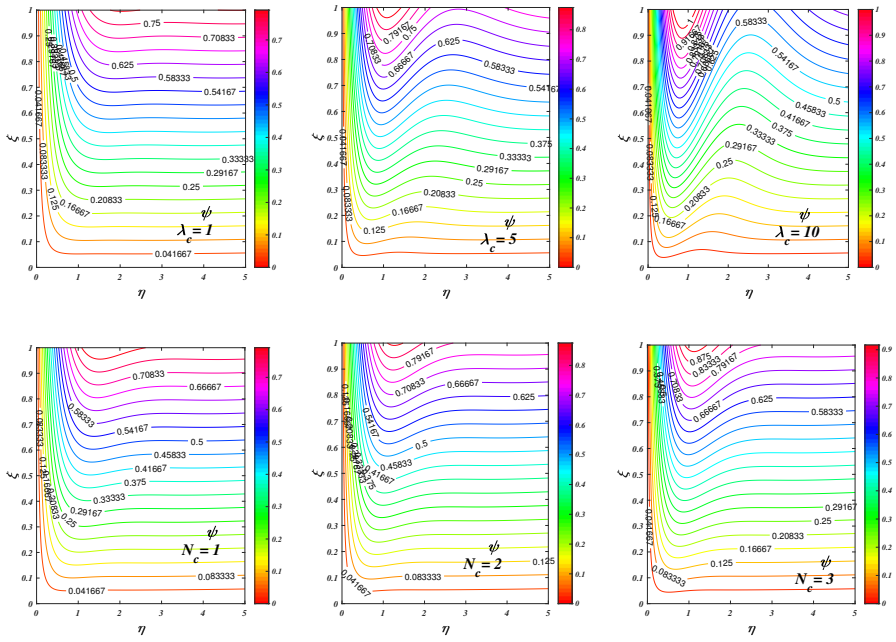

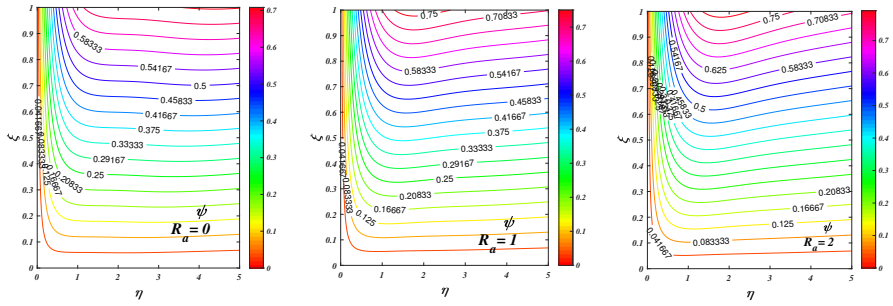

Fig. 25 Streamlines for uplifting values of λ_c, N_c and R_a.

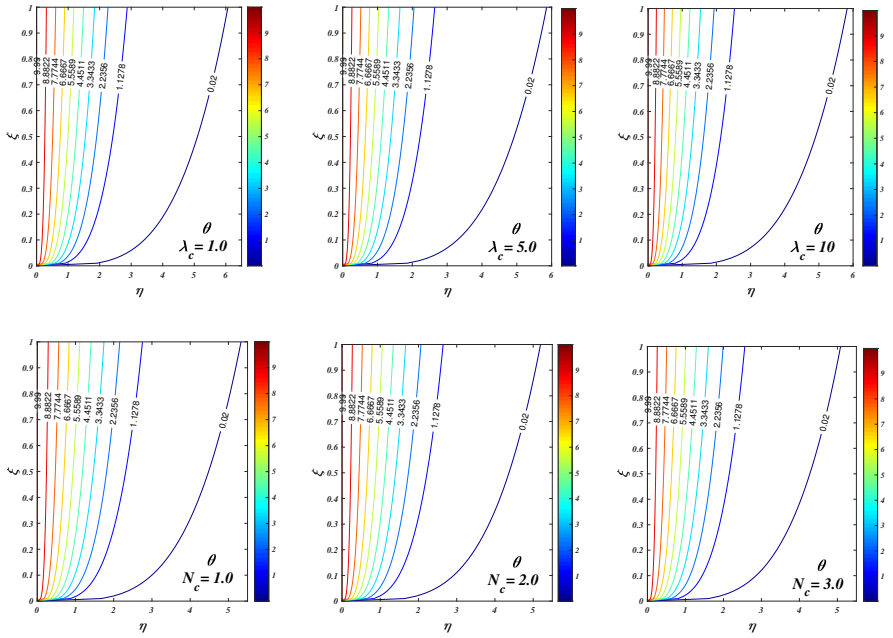

distributions diminish for amplifying the values of λ_c. Physically, higher values of convection parameter tend to enhance the convection cooling effect, as a consequence, nanofluid velocity uplifts. Further, magnification in convection cooling effect causes the decay in temperature and concentration distributions. Figures 12 and 13 are plotted to observe the f' and θ of nanofluid with increasing values of N_c. It is observed that the intensifying values of N_c uplift the nanofluid velocity but diminish the thermal related boundary thickness. This mechanism is related to the buoyancy force, thus increasing values of N_c use to strengthen the buoyancy force. This magnification in buoyancy force declines nanofluid temperature distribution. Figure 14 divulges the influence of R_a on tangent hyperbolic nanofluid temperature profiles. It is noticed that larger values of radiation lead to elevate the nanofluid temperature. The magnification

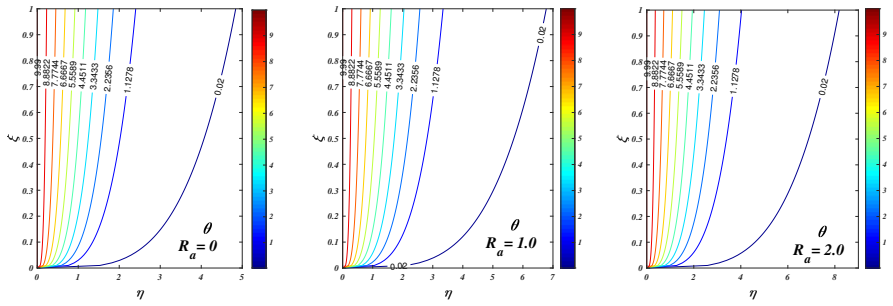

Fig. 26 Isotherms for uplifting values of λ_c, N_c and R_a.

in radiation motivates the heat transfer proceess in the tangent hyperbolic nanofluid which increase the thermal boundary layer thickness.

Figure 15 displays the results on θ for distinct values of N_T. Physically, the phenomenon of thermophoresis is related to the motion of nano-sized solid particles owing to difference in temperature distribution. Larger values of thermophoresis greatly promote the movement of nano-sized solid particles, thus nanofluid temperature rises. Figure 16 exhibits the changes in ϕ for several values of N_T. It is well known that thermophoresis has the nature to displace the nano-sized solid particles from hot place to cool place. This results in an uneven distribution in nano-size particles concentration. So that concentration profile is rising by increasing thermophoresis. The role of N_B on tangent hyperbolic nanofluid temperature is displayed in Fig. 17. As the Brownian motion enhances, the nanoparticles move freely and improperly in the fluid which in turn causes the temperature enhancement. The effect of N_B on tangent hyperbolic nanofluid concentration is exhibited in Fig. 18. Brownian motion is expressed as the ratio between mass species and nano-sized solid particles. Larger values of Brownian motion diminish the nano-sized solid particles concentration so that the nanofluid concentration decreases.

Figure 19 is drawn to explore the influence of λ_c on the skin friction factor. It is noticed that the skin friction factor is 0 at ξ= 0 and the skin friction factor is raised when ξ enhances. Moreover, an increase in mixed convection parameter augments the skin friction factor of nanofluid at the surface. Figures 20 and 21 are plotted to examine the impact of mixed convection parameter on rate of heat and mass transfer. It is observed that the rate of heat and mass transfer of nanofluid at the surface upsurge by magnifying the mixed convection. The impact of We on the skin friction factor, rate of heat and mass transfer are elucidated in Figs 22-24, respectively. It is seen that the skin friction factor at the surface enhances with an increment in We but the reverse behavior is exhibited on the rate of heat and mass transfer. It is to be noted that magnitude of rate of heat and mass transfer near the surface is higher while the rate of heat and mass transfer decline for increasing the height of

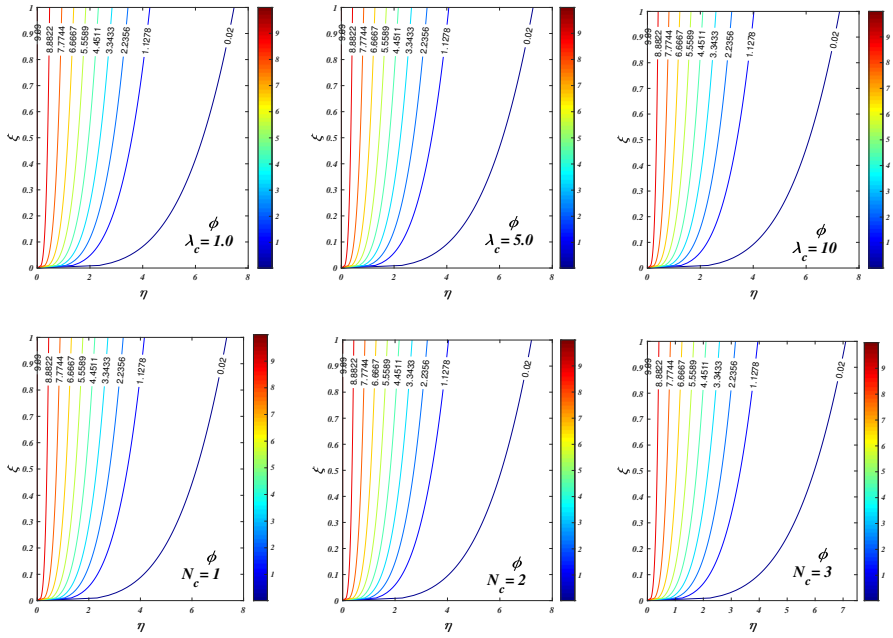

the wall.

Figures 25-27 are plotted in order to illustrate the streamlines, isotherms and isoconcentrations for various values of λ_c, N_c and R_a. The influence of λ_c, N_c and R_a on streamline is demonstrated in Fig. 25. It is observed from these figures that the streamlines are more dense near the wall at $\xi < 1$. However, streamlines manifest an oscillating nature for increasing the λ_c from 1 to 10. Moreover, for higher values of N_c and R_a, the streamlines show the oscillating nature due to the buoyancy force. Figures 26 and 27 are manifested the isotherms and isoconcentrations for distinct values of λ_c, N_c and R_a, respectively. It is noticed from these figures that isotherms and isoconcentrations thicknesses slightly decrease with an increment in λ_c and N_c. However, higher values of R_a enhance the isotherms and isoconcentrations.

4.1 **Entropy generation**

This numerical study is the analysis of entropy generation in a tangent hyperbolic non-Newtonian nanofluid over a normal surface of a circular cylinder. The future examines will exhibits entropy generation in a various non-Newtonian nanofluid (eg. Williamson, Maxwell, Jeffrey). Furthermore, the rough surface of a circular cylinder also will be taken for the analysis. Characteristics of entropy generation (N_G) and Bejan number (Be) under the impacts radiation (R_a=0.0,0.5,1.0,1.5), Brinkman number (Br=0.1,0.3,0.5,0.5),

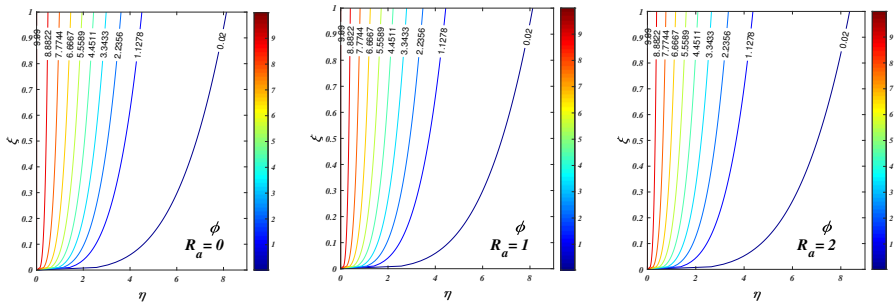

Fig. 27 Isoconcentrations for uplifting values of λ_c, N_c and R_a.

mixed convection ($\lambda_c = 1, 3, 7, 10$), dimensionless temperature ratio variable ($\alpha_T = 0.1, 0.5, 1.0, 1.5$), Eckert number ($E_c = 0.01, 0.1, 0.3, 0.5$) and thermal convection ($N_c = 0.1, 0.5, 1.0, 1.5$) are explored graphically in Figs. 28-35. Figure 28 elucidates the influence of R_a on N_G. There is an augment in N_G for raising values of R_a. As a result of R_a, the internal energy of the hyperbolic nanofluid flow system is uplifted which corresponds to enhance N_G. Figure 29 represents the effect of α_T on N_G. It is observed from this figure that there is a raise in N_G with an increment in α_T. α_T significantly controls the fluid frictional effects, thus enhances the N_G. The behavior of E_c on N_G is manifested in Fig. 30. Physically, E_c is related to self-heating mechanism of the nanofluids due to the influence of dissipation. It is seen that N_G decreases for uplifting values of E_c. Figure 31 is plotted to scrutinize the changes in N_G with increasing values of λ_c. It is evident that an increment in λ_c promotes the rate of heat transfer and generate more heat, as a consequence N_G enhances near the geometry ($\eta < 2$) but an opposite trend is manifested in the region ($4 < \eta < 4.5$). Figures 32 and 33 show the effect of N_c on N_G and Be, respectively. It can be seen that the effect of N_c enhances the total entropy generation while the reverse trend is observed on Be. As a consequence of buoyancy force, N_G and Be express this nature. Figure 34 displays N_G for varying Ψ. It is evident that increasing values of Ψ tend to lessen Be. The variation in Be with raising values of Br is manifested in Fig. 35. This figure reveals that Be decreases for uplifting values of Br. It is known that Br is the relationship between heat and molecular transport caused by fluid friction and heat transfer. Generally, Br admits viscous heating corresponding with the convective heat transfer. However, when viscous effects produce more heat which intend to control heat transport via molecular conduction. This is the reason for reduction in Be.

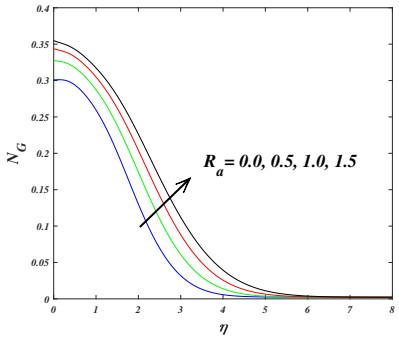

Fig. 28 N_G for uplifting values of R_a.

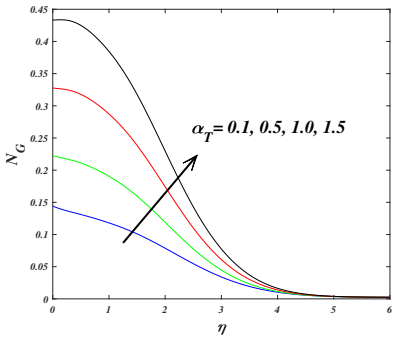

Fig. 29 N_G for uplifting values of α_T.

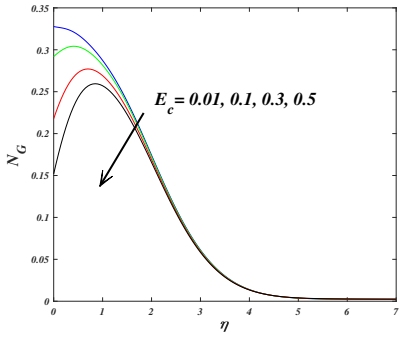

Fig. 30 N_G for uplifting values of E_c.

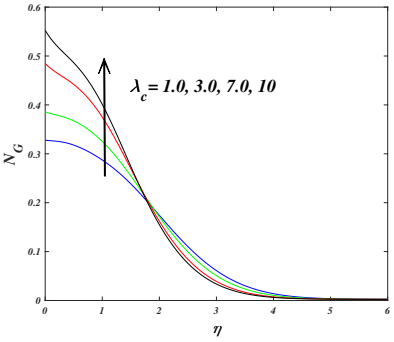

Fig. 31 N_G for uplifting values of λ_c.

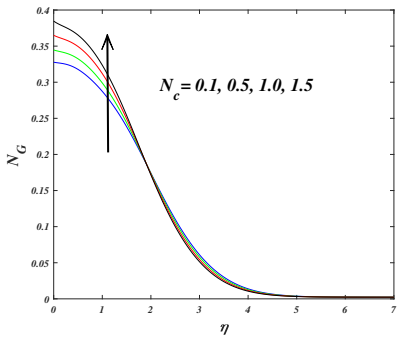

Fig. 32 N_G for uplifting values of N_c.

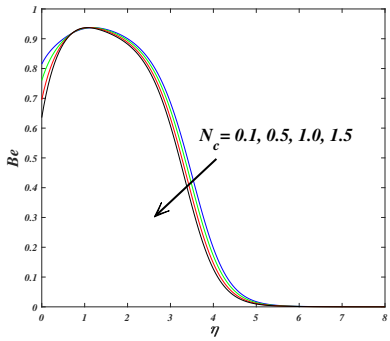

Fig. 33 Be for uplifting values of N_c.

5 Conclusion

This study has been presented to explore the heat and mass transfer characteristics and entropy analysis on hyperbolic tangent nanofluid over a circular

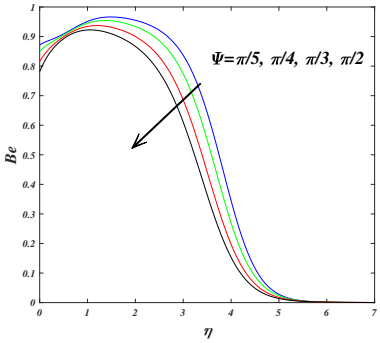

Fig. 34 Be for uplifting values of Ψ.

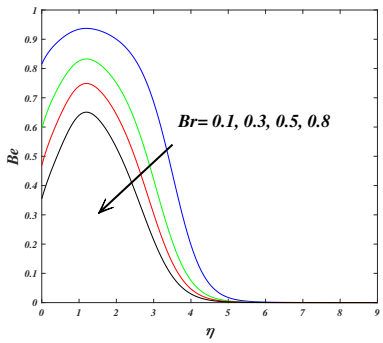

Fig. 35 Be for uplifting values of Br.

cylinder with the impacts of nonlinear Boussinesq approximation and inclined magnetic field. Non-similar variables are utilized to transform the dimensional equations into a dimensionless form which are computed by adopting an implicit finite difference KBM method. The outcomes are demonstrated in terms of a two-dimensional plot, streamlines, isotherms and isoconcentrations contours. The main findings of the current study are listed below.

- Tangent hyperbolic nanofluid velocity uplifts for enhancing the mixed convection parameter.
- The velocity and temperature distributions show an opposite nature due to the increase in thermal convection parameter.
- Temperature and concentration distributions raise with an increment in the Weissenberg number.
- The rate of heat and mass transfer at ξ=0 is higher than at ξ=1.
- Higher values of radiation, mixed convection and thermal convection parameters augment the total entropy generation.
- Magnifications in angle of inclination and Brinkman number reduce the Bejan number.
- Streamlines manifest the oscillating nature for amplifying nonlinear mixed convection.
- Isotherms and isoconcentrations boundary layers enhance for raising values of thermal radiation.

References

1. Bejan A, A study of entropy generation in fundamental convective heat transfer. J Heat Transfer. 1979;101: 718-725.
2. Ali M , Khan WA, Irfan M, Sultan F, Shahzed M , Khan M. Computational analysis of entropy generation for cross nanofluid flow. Appl Nanosci. (2019).
3. Sheikholeslami M , Ganji DD. Entropy generation of nanofluid in presence of magnetic field using Lattice Boltzmann Method. Physica A. 2014;417: 273-286.
4. Khan MI, Kumar A, Hayat T, Waqas M, Singh R. Entropy generation in flow of Carreau nanofluid. J Mol Liq. 2019;278:677-687.

5. Akbarzadeh M, Rashidi S, Keshmiri A, Shokri N. The optimum position of porous insert for a double-pipe heat exchanger based on entropy generation and thermal analysis. J Therm Anal Calorim. (2020); 139: 411-426.
6. Azadi M, Hosseinirad E, Hormozi F, Rashidi N. Second law analysis for nanofluid flow in mini-channel heat sink with finned surface: a study on fin geometries. J Therm Anal Calorim. (2020); 140: 1883-1895.
7. Shamsabadi H, Rashidi S, Esfahani JA. Entropy generation analysis for nanofluid flow inside a duct equipped with porous baffles. J Therm Anal Calorim. (2019); 135: 1009-1019.
8. Darbari B, Rashidi S, Keshmiri A. Nanofluid heat transfer and entropy generation inside a triangular duct equipped with delta winglet vortex generators. J Therm Anal Calorim. (2020);140: 1045-1055.
9. Eegunjobi AS, Makinde OD. Irreversibility Analysis of MHD Buoyancy-Driven Variable Viscosity Liquid Film along an Inclined Heated Plate Convective Cooling. J Appl Comput Mech. (2019); 5: 840-848.
10. Chamkha AJ, Selimefendigil F, Oztop HF. MHD Mixed Convection and Entropy Generation in a Lid-Driven Triangular Cavity for Various Electrical Conductivity Models. Entropy. (2018); 20: 903.
11. Selimefendigil F, Oztop HF. Effects of conductive curved partition and magnetic field on natural convection and entropy generation in an inclined cavity filled with nanofluid. Physica A. (2020); 540: 123004.
12. Alsabery AI, Selimefendigil F, Hashim I, Chamkha AJ, Ghalambaz M. Fluid-structure interaction analysis of entropy generation and mixed convection inside a cavity with flexible right wall and heated rotating cylinder. Int J Heat Mass Tran. (2019); 140: 331-345.
13. Selimefendigil F, Oztop HF, Chamkha AJ. MHD mixed convection and entropy generation of nanofluid filled lid driven cavity under the influence of inclined magnetic fields imposed to its upper and lower diagonal triangular domains. J Magn Magn Mater. (2016);406:266-281.
14. Selimefendigil F, Oztop HF. MHD mixed convection and entropy generation of power law fluids in a cavity with a partial heater under the effect of a rotating cylinder. Int J Heat Mass Tran. (2016); 98: 40-51.
15. Basha HT, Sivaraj R, Reddy AS, Chamkha AJ,Tilioua M. Impacts of temperature-dependent viscosity and variable Prandtl number on forced convective FalknerSkan flow of Williamson nanofluid. SN Appl Sci.(2020): 2;477.
16. Kumar BR, Sivaraj R. Heat and mass transfer in MHD viscoelastic fluid flow over a vertical cone and flat plate with variable viscosity. Int J Heat Mass Transf. 2013;56: 370-379.
17. Mythili D, Sivaraj R, Influence of higher order chemical reaction and non-uniform heat source / sink on Casson fluid flow over a vertical cone and flat plate. J Mol Liq. 2016;216: 466-475.
18. Gaffar SA, Ur-rehman K, Reddy PR, Prasad VR, Khan BH. Powell-Eyring fluid flow towards an isothermal sphere in a non-darcy porous medium. Can J Phys. 2019;97: 1039-1048.
19. Animasaun IL, Mahanthesh B, Sarojamma G, Damisa JS. Significance of thickness of paraboloid of revolution and buoyancy forces on the dynamics of Erying Powell fluid subject to equal diffusivity kind of quartic autocatalysis. Physica A. 2020; 124047.
20. Sivaraj R, Benazir AJ, Srinivas S, Chamkha AJ. Investigation of cross-diffusion effects on Casson fluid flow in existence of variable fluid properties. Eur Phys J Spec Top. 2019;228: 35-53.
21. Reddy GJ, Kumar M, Beg OA. Effect of temperature dependent viscosity on entropy generation in transient viscoelastic polymeric fluid flow from an isothermal vertical plate. Physica A. 2018;510:426-445.
22. Prasad VR, Kumar BR. Non-Similar Comutational Solutions for Double-Di usive MHD Transport Phenomena for Non-Newtnian Nanofluid From a Horizontal Circular Cylinder. Nonlinear Eng. 2019;8:470-485.
23. Gaffar SA, Prasad VR, Beg OA, Numerical study of flow and heat transfer of non-Newtonian Tangent Hyperbolic fluid from a sphere with Biot number effects. Alexandria Eng J. 2015; 54: 829-841.

24. Khan MI, Khan TA, Qayyum S, Hayat T, Khan MI, Alsaedi A. Entropy generation optimization and activation energy in nonlinear mixed convection flow of a tangent hyperbolic nanofluid. Eur Phys J Plus. 2018; 133:329.
25. Nayak MK, Sen SS, Shaw S, Makinde OD, Chamkha AJ. Investigation of Partial Slip and Viscous Dissipation Effects on the Radiative Tangent Hyperbolic Nanofluid Flow Past a Vertical Permeable Riga Plate with Internal Heating: Bungiorno Model. J Nanofluid. 2019; 1-12.
26. Vasu B, Gorla RSR, Beg OA, Murthy PVSN, Prasad VR, Kadir A. Unsteady Flow of a Nanofluid over a Sphere with Nonlinear Boussinesq Approximation. J Thermophys Heat Transf. 2019; 33:1-13.
27. Mahanthesh B, Gireesha BJ, Thammanna GT, Shehzad SA, Abbasi FM, Gorla RSR. Nonlinear convection in nano Maxwell fluid with nonlinear thermal radiation: A three-dimensional study. Alexandria Eng J. 2018;57:1927-1935.
28. Waqas M, Dogonchi AS, Shehzad SA, Khan MI, Hayat T, Alsaedi A. Nonlinear convection and joule heating impacts in magneto-thixotropic nano fl uid strati fi ed fl ow by convectively heated variable thicked surface. J Mol Liq. 2020;300: 111945.
29. Patil PM, Shashikant A, Hiremath PS. Diffusion of liquid hydrogen and oxygen in nonlinear mixed convection nanofluid flow over vertical cone. Int J Hydrogen Energy. 2019;44 : 17061-17071.
30. Kameswaran PK, Sibanda P, Partha MK, Murthy PVSN. Thermophoretic and Nonlinear Convection in Non-Darcy Porous Medium. J Heat Transfer. 2015;136: 1-9.
31. Choi SUS, and Eastman JA, Enhancing thermal conductivity of fluids with nanoparticles. In: Proceedings of the 1995 ASME international mechanical engineering congress and exposition, 1217 November (American Society of Mechanical Engineers, fluids engineering division (publication) FED, 1995). (1995); 231: 99-105.
32. Nazari S, Ellahi R, Sarafraz MM, Safaei MR, Asgari A, Akbari OA. Numerical study on mixed convection of a non-Newtonian nanofluid with porous media in a two lid-driven square cavity. J Therm Anal Calorim. (2020);140:1121-1145.
33. Khan LA, Raza M, Mir NA, Ellahi R. Effects of different shapes of nanoparticles on peristaltic flow of MHD nanofluids filled in an asymmetric channel. J Therm Anal Calorim. (2020); 140: 879-890.
34. Hong K, Yang Y, Rashidi S, Guan Y, Xiong Q. Numerical simulations of a Cuwater nanofluid-based parabolic-trough solar collector. J Therm Anal Calorim. (2020); https://doi.org/10.1007/s10973-020-09386-4.
35. Raza M, Ellahi R, Sait, SM, Sarafraz MM, Shadloo MS, Waheed I. Enhancement of heat transfer in peristaltic flow in a permeable channel under induced magnetic field using different CNTs. J Therm Anal Calorim. (2020):140; 1277-1291.
36. Akar S, Rashidi S, Esfahani JA, Karimi N. Targeting a channel coating by using magnetic field and magnetic nanofluids. J Therm Anal Calorim. (2019);137: 381-388.
37. Tiwari RJ, Das MK. Heat transfer augmentation in a two-sided lid-driven differentially heated square cavity utilizing nanofluids. Int. J. Heat. Mass Transf., (2007); 50:2002-2018.
38. Buongiorno J. Convective transport in nanofluids. J Heat Transfer. (2006); 128:240.
39. Rashad AM, Chamkha AJ, Modather M. Mixed convection boundary-layer flow past a horizontal circular cylinder embedded in a porous medium filled with a nanofluid under convective boundary condition. Comput Fluids. 2013;86: 380-388.
40. Merkin JH. Free convection boundary layers on cylinders of elliptic cross section, J Heat Transfer. 1977;99: 453-457.
41. Yih KA. Effect of blowing/suction on MHD-natural convection over horizontal cylinder: UWT or UHF, Acta Mech. 2000;144: 17-27.
42. Cebeci T, Pradshaw P. Physical and Computational Aspects of Convective Heat Transfer,Springer,New York, 1998.

Table 3 Impacts of N_r and E_c on local skin friction coefficient $\left(C_f^*\right)$, dimensionless local rate of heat transfer (Nu^*) and dimensionless local rate of mass transfer (Sh^*) for various values of ξ.

Physical Parameters	Values	Physical Quantities	ξ						CPU time(Sec.)
			0	0.2	0.4	0.6	0.8	1.0	
N_r	0.1	C_f^*	0	0.3984	0.7626	1.0709	1.3065	1.4599	11.438911
		Nu^*	1.1194	1.1090	1.0884	1.0580	1.0185	0.9706	
		Sh^*	0.8418	0.8354	0.8226	0.8036	0.7784	0.7473	
	0.3	C_f^*	0	0.3829	0.7321	1.0261	1.2489	1.3907	11.858886
		Nu^*	1.1146	1.1042	1.0835	1.0529	1.0131	0.9649	
		Sh^*	0.8356	0.8291	0.8161	0.7968	0.7712	0.7395	
	0.5	C_f^*	0	0.3672	0.7013	0.9810	1.1906	1.3208	11.161408
		Nu^*	1.1097	1.0992	1.0783	1.0475	1.0075	0.9589	
		Sh^*	0.8291	0.8225	0.8093	0.7897	0.7636	0.7314	
	0.7	C_f^*	0	0.3515	0.6703	0.9356	1.1318	1.2502	11.189030
		Nu^*	1.1046	1.0940	1.0730	1.0420	1.0016	0.9527	
		Sh^*	0.8225	0.8158	0.8023	0.7823	0.7557	0.7228	
E_c	0.01	C_f^*	0	0.3984	0.7626	1.0709	1.3065	1.4599	11.438911
		Nu^*	1.1194	1.1090	1.0884	1.0580	1.0185	0.9706	
		Sh^*	0.8418	0.8354	0.8226	0.8036	0.7784	0.7473	
	0.1	C_f^*	0	0.3674	0.7021	0.9833	1.1952	1.3288	11.072150
		Nu^*	1.1097	1.0888	1.0475	0.9885	0.9154	0.8332	
		Sh^*	0.8291	0.8230	0.8108	0.7926	0.7682	0.7378	
	0.3	C_f^*	0	0.3677	0.7038	0.9883	1.2057	1.3468	11.256386
		Nu^*	1.1097	1.0656	0.9786	0.8558	0.7068	0.5453	
		Sh^*	0.8291	0.8241	0.8142	0.7991	0.7787	0.7525	
	0.5	C_f^*	0	0.3680	0.7056	0.9934	1.2163	1.3653	11.169868
		Nu^*	1.1097	1.0424	0.9092	0.7210	0.4927	0.2452	
		Sh^*	0.8291	0.8252	0.8175	0.8057	0.7894	0.7677	

Table 4 Impacts of N_T and N_B on local skin friction coefficient $\left(C_f^*\right)$, dimensionless local rate of heat transfer (Nu^*) and dimensionless local rate of mass transfer (Sh^*) for various values of ξ.

Physical Parameters	Values	Physical Quantities	ξ						CPU time(Sec.)
			0	0.2	0.4	0.6	0.8	1.0	
N_T	0.01	C_f^*	0	0.3675	0.7019	0.9819	1.1917	1.3221	10.986395
		Nu^*	1.1192	1.1086	1.0876	1.0566	1.0162	0.9673	
		Sh^*	0.8428	0.8361	0.8226	0.8025	0.7760	0.7431	
	0.1	C_f^*	0	0.3672	0.7013	0.9810	1.1906	1.3208	11.788723
		Nu^*	1.1097	1.0992	1.0783	1.0475	1.0075	0.9589	
		Sh^*	0.8291	0.8225	0.8093	0.7897	0.7636	0.7314	
	0.3	C_f^*	0	0.3666	0.7001	0.9793	1.1884	1.3183	11.129852
		Nu^*	1.0889	1.0786	1.0581	1.0278	0.9884	0.9407	
		Sh^*	0.8016	0.7953	0.7826	0.7637	0.7387	0.7077	
	0.5	C_f^*	0	0.3661	0.6991	0.9778	1.1865	1.3160	10.991573
		Nu^*	1.0687	1.0585	1.0384	1.0086	0.9699	0.9229	
		Sh^*	0.7778	0.7717	0.7595	0.7414	0.7172	0.6872	
N_B	0.3	C_f^*	0	0.3672	0.7013	0.9810	1.1906	1.3208	10.967421
		Nu^*	1.1097	1.0992	1.0783	1.0475	1.0075	0.9589	
		Sh^*	0.8291	0.8225	0.8093	0.7897	0.7636	0.7314	
	0.5	C_f^*	0	0.3679	0.7026	0.9829	1.1929	1.3236	11.181454
		Nu^*	1.0769	1.0667	1.0465	1.0166	0.9777	0.9306	
		Sh^*	0.8369	0.8303	0.8169	0.7971	0.7708	0.7382	
	0.7	C_f^*	0	0.3684	0.7035	0.9843	1.1947	1.3258	11.330983
		Nu^*	1.0449	1.0350	1.0153	0.9863	0.9485	0.9028	
		Sh^*	0.8405	0.8337	0.8204	0.8004	0.7740	0.7414	
	0.9	C_f^*	0	0.3688	0.7045	0.9856	1.1964	1.3277	11.356811
		Nu^*	1.0136	1.0040	0.9849	0.9567	0.9200	0.8756	
		Sh^*	0.8425	0.8358	0.8224	0.8024	0.7760	0.7433	